Variation in Global Chemical Composition of PM$_{2.5}$: Emerging Results from SPARTAN

Graydon Snider[1], Crystal L. Weagle[2], Kalaivani K. Murdymootoo[1], Amanda Ring[1], Yvonne Ritchie[1], Emily Stone[1], Ainsley Walsh[1], Clement Akoshile[3], Nguyen Xuan Anh[4], Rajasekhar Balasubramanian[5], Jeff Brook[6], Fatimah D. Qonitan[7], Jinlu Dong[8], Derek Griffith[9], Kebin He[7], Brent N. Holben[10], Ralph Kahn[9], Nofel Lagrosas[11], Puji Lestari[6], Zongwei Ma[12], Amit Misra[13], Leslie K. Norford[14], Eduardo J. Quel[15], Abdus Salam[16], Bret Schichtel[17], Lior Segev[18], S.N. Tripathi[12], Chien Wang[19], Chao Yu[20], Qiang Zhang[7], Yuxuan Zhang[7], Michael Brauer[21], Aaron Cohen[22], Mark D. Gibson[23], Yang Liu[18], J. Vanderlei Martins[24], Yinon Rudich[16], Randall V. Martin*[1,2,25]

---

[*]Corresponding author email: graydon.snider@dal.ca or randall.martin@dal.ca phone: 902-494-1820, fax: 902-494-5191

Affiliations
[1]Department of Physics and Atmospheric Science, Dalhousie University, Halifax, Canada

[2]Department of Chemistry, Dalhousie University, Halifax, Canada

[3]Department of Physics, University of Ilorin, Ilorin, Nigeria

[4]Institute of Geophysics, Vietnam Academy of Science and Technology, Hanoi, Vietnam

[5]Department of Civil and Environmental Engineering, National University of Singapore

[6]Department of Public Health Sciences, University of Toronto, Toronto, Ontario, Canada M5S 1A8

[7] Faculty of Civil and Environmental Engineering, ITB, JL. Ganesha No.10, Bandung 40132, Indonesia

[8]Center for Earth System Science, Tsinghua University, Beijing, China

[9]Council for Scientific and Industrial Research (CSIR), Pretoria, South Africa

[10]Earth Science Division, NASA Goddard Space Flight Center, Greenbelt, Maryland, USA

[11]Manila Observatory, Ateneo de Manila University campus, Quezon City, Philippines

[12] School of Environment, Nanjing University, Nanjing, China.

[13] Center for Environmental Science and Engineering, Indian Institute of Technology Kanpur, India

[14] Department of Architecture, Massachusetts Institute of Technology, Cambridge, MA, 02139, USA

[15]UNIDEF (CITEDEF-CONICET) Juan B. de la Salle 4397 – B1603ALO Villa Martelli, Buenos Aires, Argentina

[16]Department of Chemistry, University of Dhaka, Dhaka - 1000, Bangladesh

[17] Cooperative Institute for Research in the Atmosphere, Colorado State, Colorado, USA

[18] Department of Earth and Planetary Sciences, Weizmann Institute, Rehovot 76100, Israel

[19]Center for Global Change Science, Massachusetts Institute of Technology, Cambridge, MA, 02139, USA

[20]Rollins School of Public Health, Emory University, 1518 Clifton Road NE, Atlanta, GA 30322, United States

[21]School of Population and Public Health, University of British Columbia, Vancouver, British Columbia, Canada

[22]Health Effects Institute, 101 Federal Street Suite 500, Boston, MA 02110-1817, USA

[23]Department of Process Engineering and Applied Science, Dalhousie University, Halifax, Canada,

[24]Department of Physics and Joint Center for Earth Systems Technology, University of Maryland, Baltimore County, Baltimore, Maryland, USA

[25]Harvard-Smithsonian Center for Astrophysics, Cambridge, MA 02138, USA

Abstract

The Surface PARTiculate mAtter Network (SPARTAN) is a long-term project that includes characterization of chemical and physical attributes of aerosols from filter samples collected worldwide. This manuscript discusses the ongoing efforts of SPARTAN to define and quantify major ions and trace metals found in fine particulate matter ($PM_{2.5}$). Our methods infer the spatial and temporal variability of $PM_{2.5}$ in a cost-effective manner. Gravimetrically-weighed filters represent multi-day averages of $PM_{2.5}$, with a collocated nephelometer sampling air continuously. SPARTAN instruments are paired with AErosol RObotic NETwork (AERONET) sun photometers to better understand the relationship between ground-level $PM_{2.5}$ and columnar aerosol optical depth (AOD).

We have examined the chemical composition of $PM_{2.5}$ at 12 globally dispersed, densely populated urban locations and a site at Mammoth Cave (US) National Park used as a background comparison. Each SPARTAN location has so far been active between the years 2013 and 2016 over 2 to 26 month periods, with an average period of 12 months per site. These sites have collectively gathered over 10 site-years of quality aerosol data. The major $PM_{2.5}$ constituents across all sites (relative contribution ± SD) are ammoniated sulfate (20% ± 11%), crustal material (13.4% ± 9.9%), black carbon (11.9% ± 8.4%), ammonium nitrate (4.7% ± 3.0%), sea salt (2.3% ± 1.6%), trace element oxides (1.0% ± 1.1%), water (7.2% ± 3.3%) at 35% RH, and residual matter (40% ± 24%).

Analysis of filter samples reveals that several $PM_{2.5}$ chemical components varied by more than an order of magnitude between sites. Ammoniated sulfate ranges from 1.1 μg m^{-3} (Buenos Aires, Argentina) to 17 μg m^{-3} (Kanpur, India [dry season]). Ammonium nitrate ranged from 0.2 μg m^{-3} (Mammoth Cave, in summer) to 6.8 μg m^{-3} (Kanpur, dry season). Equivalent black carbon ranged from 0.7 μg m^{-3} (Mammoth Cave) to over 8 μg m^{-3} (Dhaka, Bangladesh and Kanpur, India). Comparison of SPARTAN versus coincident measurements from the Interagency Monitoring of Protected Visual Environments (IMPROVE) network at Mammoth Cave yielded a high degree of consistency for daily $PM_{2.5}$ ($r^2 = 0.76$, slope = 1.12), daily sulfate ($r^2 = 0.86$, slope = 1.03) and mean fractions of all major $PM_{2.5}$ components (within 6%). Major ions generally agree well with previous studies at the same urban locations (e.g. sulfate fractions agree within 4% for eight out of 11 collocation comparisons). Enhanced anthropogenic dust fractions in large urban areas (e.g. Singapore, Kanpur, Hanoi and Dhaka) are apparent from high Zn:Al ratios.

The expected water contribution to aerosols is calculated via the hygroscopicity parameter κ_v for each filter. Mean aggregate values ranged from 0.15 (Ilorin) to 0.28 (Rehovot). The all-site parameter mean is 0.20 ± 0.04. Chemical composition and water retention in each filter measurement allows inference of hourly $PM_{2.5}$ at 35% relative humidity by merging with nephelometer measurements. These hourly $PM_{2.5}$ estimates compare favorably with a beta attenuation monitor (MetOne) at the nearby US embassy in Beijing, with a coefficient of variation $r^2 = 0.67$ ($n = 3167$), compared to $r^2 = 0.62$ when κ_v was not considered. SPARTAN continues to provide an open-access database of $PM_{2.5}$ compositional filter information and hourly mass collected from a global federation of instruments.

1. Introduction

Fine particulate matter with a median aerodynamic diameter less than, or equal to, 2.5 μm ($PM_{2.5}$), is a robust indicator of premature mortality (Chen et al., 2008; Laden et al., 2006). Research on long-term exposure to ambient $PM_{2.5}$ has documented serious adverse health effects, including increased mortality from chronic cardiovascular disease, respiratory disease, and lung cancer (WHO, 2005). Outdoor fine particulate matter ($PM_{2.5}$) is recognized as a significant air pollutant, with an Air Quality Guideline set by the WHO at 10 μg m^{-3} annual average (WHO, 2006). Many regions of the world far exceed these long-term recommendations (Brauer et al., 2015; van Donkelaar et al., 2015), and the impact on health is substantial. The 2013 Global Burden of Disease estimated that outdoor $PM_{2.5}$ caused 2.9 million deaths (3 % of all deaths) and 70 million years of lost healthy life on a global scale (Forouzanfar et al., 2015). Atmospheric aerosol is also the most uncertain agent contributing to radiative forcing of climate change (IPCC, 2013). Aerosol mass and composition also play a critical role in atmospheric visibility (Malm et al. 1994). Additional observations are needed to improve the concentration estimates for $PM_{2.5}$ as a global risk factor, and to better understand the chemical components and sources contributing to its formation.

The chemical composition of $PM_{2.5}$ offers valuable information to identify the contributions of specific sources, and to understand aerosol properties and processes that could affect health, climate and atmospheric conditions. Spatial mapping of aerosol type and composition using satellite observations and chemical transport modelling can help elucidate the global exposure burden of fine particulate matter composition (Kahn and Gaitley, 2015; Lelieveld et al., 2015; Patadia et al., 2013; Philip et al., 2014a), however ground-level sampling remains necessary to evaluate these estimates and provide quantitative detail. Furthermore, the long-term health impacts of specific chemical components are not well understood (e.g. Lepeule et al., 2012). The health-related impacts of specific PM composition have been reviewed previously (Lippmann, 2014). Although $PM_{2.5}$ composition can be implicated in the variance observed in cardiovascular health effects, there is insufficient long-term $PM_{2.5}$ characterization for adequate health impact assessments of specific aerosol mixtures (e.g. Bell et al., 2007). More generally, urban $PM_{2.5}$ speciation is not yet consistently characterized on a global scale. Continental sampling has been conducted in North America (Hand et al., 2012) and Europe (Putaud et al., 2004, 2010), however there remains a need for a global network that consistently measures $PM_{2.5}$ chemical composition in densely populated regions.

No global $PM_{2.5}$ protocol exists for relative humidity (RH) filter equilibration. The U.S. EPA measurements are between 30-40% RH, European measurements are below 50% RH, and different protocols exist elsewhere. Ambient humidity affects the relationship of dry $PM_{2.5}$ with satellite observations of aerosol optical depth. Aerosol water also influences the relationship between dry $PM_{2.5}$ and aerosol scatter. A large body of literature has examined the relationship of aerosol composition with hygroscopicity (e.g. IMPROVE (Hand et al., 2012; IMPROVE, 2015), Chemical Species Network (CSN) (Chu, 2004; USEPA, 2015), ISORROPIA (Fountoukis and Nenes, 2007), and Aerosol Inorganic Model (AIM) (Wexler and Clegg, 2002)). More recently Petters and Kreidenweis (2007, 2008, 2013) have developed κ-Kohler theory, which assigns individual hygroscopicity parameters κ to all major components, from insoluble crustal materials to sea-salt. Mixed values can then be weighted by local aerosol composition.

106
107   Ground-based observations of $PM_{2.5}$ have insufficient coverage at the global scale to
108   provide assessment of long-term human exposure. Satellite remote sensing offers a promising
109   means of providing an extended temporal record to estimate population exposure to $PM_{2.5}$ on a
110   global scale, and especially for areas with limited ground-level $PM_{2.5}$ measurements (Brauer et
111   al., 2015; van Donkelaar et al., 2015). Even in areas where monitor density is high, satellite-
112   based estimates provide additional useful information on spatial and temporal patterns in air
113   pollution (Kloog et al., 2011, 2013; Lee et al., 2012). However, there are outstanding questions
114   about the accuracy and precision with which ground-level aerosol mass concentrations can be
115   inferred from satellite remote sensing. Standardized $PM_{2.5}$ measurements, collocated with
116   ground-based measurements of aerosol optical depth, are needed to evaluate and improve $PM_{2.5}$
117   estimates from satellite remote sensing. To meet these sampling needs, the ground-based
118   network SPARTAN (Surface PARTiculate mAtter Network) is designed to evaluate and enhance
119   satellite-based estimates of $PM_{2.5}$ by measuring fine particle aerosol concentrations and
120   composition continuously over multi-year periods at sites where aerosol optical depth is also
121   measured (Holben et al., 1998; Snider et al., 2015). The network includes air filter sampling and
122   nephelometers that together provide long-term and hourly $PM_{2.5}$ estimates at low RH (35%).
123
124   We discuss the ongoing efforts of the SPARTAN project to quantify major ions and trace
125   metals found in aerosols worldwide. Section 2 describes the methodology used to infer $PM_{2.5}$
126   composition. Section 3 defines categories of aerosol types (crustal and residual material, black
127   carbon, ammonium nitrate, ammoniated sulfate, sea salt, and trace metal oxides) as a function of
128   specific chemical species. Section 4 describes the implementation of sub-saturated κ-Kohler
129   theory to estimate aerosol water content based on aerosol compositional information. Section 5
130   compares relative aerosol composition with that reported in available literature, and assesses the
131   general consistency of our findings across all sites. Section 6 evaluates hourly $PM_{2.5}$ estimates
132   (35% RH) at Beijing with a beta attenuation monitor at the US Embassy.
133

2. Overview of Methodology

135
136   SPARTAN has been collecting $PM_{2.5}$ on PTFE filters for at least two months, across 13
137   SPARTAN sites, between 2013 and 2016, with an average period of 12 months per site. Snider
138   et al. (2015) provide an overview of the SPARTAN PM observation network, the cost-effective
139   sampling methods employed and post sampling instrumental methods of analysis. Each site
140   utilizes a combination of continuous monitoring by nephelometry and mass concentration via
141   filter-based sampling. Nephelometer scatter is averaged to hourly intervals at three wavelengths
142   (457nm, 520nm, 634nm), and converted to 550 nm via a fitted Angstrom exponent. Total scatter
143   is proportional to $PM_{2.5}$ mass and volume (Chow et al., 2006). Hence we provide dry (35% RH)
144   hourly $PM_{2.5}$ estimates by combining scatter at 550 nm at ambient RH with filter mass and
145   chemical composition information used to determine water content as described below.
146
147   Briefly, filter-based measurements are collected with an AirPhoton SS4i automated air
148   sampler. Each sampler houses a removable filter cartridge that protects seven sequentially active
149   25 mm diameter filters plus a field blank. Air samples first pass through a bug screen and then a
150   greased impactor plate to remove particles larger than 10 μm in diameter. Aerosols are collected
151   in sequence on a preweighed Nuclepore filter membrane (8 μm, SPI) that removes coarse-mode

152 aerosols with diameters from 2.5 - 10 μm in diameter (PM$_c$), while fine aerosols (PM$_{2.5}$) are then
153 collected on pre-weighed PTFE filters (2 μm, SKC). For each filter, sampling is timed at regular,
154 staggered 24-hour intervals throughout a 9-day period. Sampling ends for each filter at 09:00
155 when temperatures are low, to reduce loss of semi-volatile components. As described by Snider
156 et al (2015), loss rates of ammonium nitrate during passive air flow were an order of magnitude
157 less than during active air flow. Thus the sampling protocol is designed to actively sample for
158 one diurnal cycle and to avoid daytime sampling after collecting nighttime PM. Following the
159 IMPROVE protocol (Hand and Malm, 2006), filters are transported at room temperature in
160 sealed containers between measurement sites and the central SPARTAN laboratory at Dalhousie
161 University, where analysis is conducted.
162
163   Site locations are designed to sample under a variety of conditions, including biomass
164 burning, (e.g. West Africa and South America), biofuel emissions (e.g. South Asia), monsoonal
165 conditions (e.g. West Africa and Southeast Asia), suspended mineral dust (e.g. West Africa and
166 the Middle East) and urban crustal material. Each SPARTAN site provides a representative
167 example of local and regional conditions in highly populated areas. Site selection prioritizes
168 under-represented globally-dispersed, population-dense regions; no SPARTAN sites yet exist in
169 Europe. The sites of Atlanta and Mammoth Cave are included for instrument inter-comparison
170 purposes with other networks.

171   ## 2.1. Filter weighing

172 Filters (PTFE, capillary) are both pre and post-weighed in triplicate using a Sartorius Ultramicro
173 balance with 0.1 μg precision. Gravimetric weighing is performed in a cleanroom facility at 35 ±
174 5% RH and 20-23°C. A total of 497 quality-controlled filters have been weighed across all
175 SPARTAN sites. The median collected material on sampled filters, as well as the lower and
176 upper quintiles (in parentheses), are 72 (42, 131) μg for Teflon and 90 (44, 154) μg for
177 Nuclepore. The combined uncertainty (± 2σ) of quality-assured single filter PM mass
178 measurements is ± 4.0 μg. These filters are subsequently analyzed for water-soluble ions, trace
179 metals, and surface reflectance to obtain black carbon.

180   ## 2.2. Equivalent Black Carbon (EBC)

181 We define the equivalent black carbon (EBC) as the black carbon content of PTFE filters derived
182 via surface reflectance R using the Diffusion Systems Smoke Stain Reflectometer EEL 43M
183 (Quincey et al., 2009) as further discussed in Sect. 4.6. We use the term equivalent black carbon
184 following the recommendation of Petzold et al. (2013) for data derived from optical absorption
185 methods.

186   ## 2.3. Trace metals

187 To maximize the information extracted from the filters, each one is cut in half with a ceramic
188 blade following approaches similar to Zhang et al. (2013) and Gibson et al. (2009). One filter
189 half is analyzed for relevant trace metals, i.e. crustal components Zn, Mg, Fe, and Al. We digest
190 this half by adding it to 3.0 mL of 7% trace metal grade nitric acid, similar to Fang et al. (2015).
191 The acid/filter combination is boiled at 97°C for 2 hours, and the liquid extract is submitted for
192 quantitative analysis via inductively coupled plasma mass spectrometry (ICP-MS, Thermo
193 Scientific X-Series 2).

 ### 2.4. Water soluble ions

Water-soluble ions $NO_3^-, SO_4^{2-}, NH_4^+,\ K^+, Na^+$ are detected using the second filter half. The filter is spiked with 120 μL of isopropyl alcohol and immersed in 2.9 mL of 18 MΩ Milli-Q water. Filters and liquid extracts are sonicated together for 25 min before being passed through a 0.45 μm membrane filter to remove larger matrix components. Extractions are analyzed by ion chromatography (IC) via a Thermo Dionex ICS-1100 instrument (anions) and a Thermo Dionex ICS-1000 (cations) instrument (Gibson et al., 2013a, 2013b).

3. PM$_{2.5}$ aerosol composition

Section 2 defined the methodology of basic physical and chemical properties obtained in SPARTAN filters. Section 3 describes the chemical definitions used to infer each chemical component as discussed in turn below. Table 1 contains a summary of equations and accompanying references used to quantify SPARTAN PM$_{2.5}$ chemical composition.

3.1. Sea Salt (SS)

We take 10% of [Al] to be associated with Na and remove this crustal sodium component (Remoundaki et al., 2013). Sea salt is then represented as 2.54[Na$^+$]$_{ss}$ to account for the associated [Cl$^-$] (Malm et al., 1994).

3.2. Ammonium nitrate (ANO₃)

We treat all nitrate as neutralized by ammonium as NH$_4$NO$_3$. The corresponding mass of ANO$_3$ is a 1:1 molar ratio of NH$_4$:NO$_3$, or 1.29[NO$_3^-$] based on molecular weight.

3.3. Sodium sulfate (Na₂SO₄)

Sodium sulfate is treated as a fraction of measured sodium, 0.18[Na$^+$]$_{SS}$ (Henning et al., 2003); however, it contributes negligibly to total aerosol mass (< 0.1%) at all sites.

3.4. Ammoniated sulfate (ASO₄)

Ammonium not associated with nitrate, and sulfate not associated with sodium, are assumed to mutually associate as a mixture of NH$_4$HSO$_4$ and (NH$_4$)$_2$SO$_4$.

3.5. Crustal material (CM)

Crustal material consists of re-suspended road dust, desert dust, soil, and sand. Following the elemental composition of natural desert dusts by Wang (2015), we generalize that natural CM is approximately 10×[Al + Fe + Mg]. Aluminum, iron, and magnesium are chosen due to their collectively consistent composition in natural mineral dust and frequency above detection limit (> 95%). Silicon is not available. Titanium was found not to contribute significantly (< 1%) to CM mass.

3.6. Equivalent Black Carbon (EBC)

The amount of EBC carbon (μg) is logarithmically related to concentration, as determined by relative surface reflectance R/R_0. For a given exposed filter area, absorption cross-section and light path, reflectance is related to concentration via

$$[EBC] = \frac{-A}{qv} \ln\left(\frac{R}{R_0}\right) \qquad \text{Eq. 1}$$

232   where v is volume of air (0.9 to 5.8 m^3), A is the filter surface area (3.1 cm^2), and q is the product
233   of the effective reflectivity path p and mass-specific absorption cross section σ_{SSR} (cm^2/μg). The
234   absorption coefficient σ_{SSR} used here is 0.06 cm^2/μg based on prior literature (Barnard et al.,
235   2008; Bond and Bergstrom, 2006), adjusted to the 620 nm detection peak of the SSR. The
236   effective light path p here is taken to be 1.5 for our thick PTFE filters (e.g. Taha et al., 2007). We
237   treat water uptake by EBC as negligible.

3.7. Trace elemental oxides (TEO)

239   Trace elemental oxides are the summation of oxides for all measured ICP trace elements, and
240   make up a negligible portion of total mass (< 1%). We include these concentrations for
241   completeness. Water uptake by TEO is treated as negligible.

3.8. Particle-bound water (PBW) associated with inorganics

243   We estimate the water-mass uptake for the inorganic chemical components of sea salt (SS),
244   ammonium nitrate (ANO$_3$) and ammoniated sulfate (ASO$_4$). The mass of particle-bound water
245   (PBW) associated with chemical component X is

$$PBW_X = [X]\kappa_{m,X}\frac{RH}{100 - RH} \qquad \text{Eq. 2}$$

246   The total mass of inorganic (IN) PBW is then $PBW_{IN} = \sum_X PBW_X$.

3.9. Residual matter (RM)

248   Residual matter, which is treated as mainly organics, is estimated by subtracting dry inorganic
249   mass (IN) and its associated water (referenced to our weighing conditions of 35 ± 5 % RH) from
250   total PM$_{2.5}$ mass:

$$RM_{35\%} = PM_{2.5,35\%} - [IN] - [PBW_{IN}] \qquad \text{Eq. 3}$$

251   Negative RM$_{35\%}$ values are retained if reconstructed inorganic mass at 35% RH exceeds total
252   PM$_{2.5}$ by less than 10%, otherwise values are flagged and excluded from the mass average.
253   Negative values occur, on average, 2% of the time. Water-free RM (0% RH) is estimated by
254   subtracting organic-associated PBW using an estimated hygroscopic parameter $\kappa_{m,RM} = 0.1$ as
255   discussed in section 4.
256

4. Aerosol hygroscopicity

258
259   We apply the single-parameter measure of aerosol hygroscopicity (κ) developed by Petters
260   and Kreidenweis (2007, 2008, 2013) to represent the contribution of water uptake by individual
261   components. The κ parameter is defined from 0 (insoluble materials) to greater than 1 for sea
262   salt. Although initially developed for supersaturated CCN conditions, hygroscopic parameters κ
263   have been more recently used in sub-saturated conditions (Chang et al., 2010; Dusek et al., 2011;
264   Giordano et al., 2013; Hersey et al., 2013). For particle diameters that dominate the mass fraction
265   of PM$_{2.5}$ (larger than 50 nm), the difference in κ between CCN and sub-saturated aerosols is

266 small (Dusek et al., 2011). The water retention of internal mixtures of aerosol components is
267 often predicted within experimental error (Kreidenweis et al., 2008). Aged, polarized organic
268 material, which is a major component of $PM_{2.5}$, shows comparable growth factors both in super-
269 and sub-saturated regions (Rickards et al., 2013).
270
271   The volume hygroscopicity parameter κ_v is defined as a function of particle volume V and
272 water activity a_w

$$\frac{1}{a_w} = 1 + \kappa_v \frac{V_d}{V_w} \qquad\qquad \text{Eq. 4}$$

273 where V_d and V_w are the dry particulate matter and water volumes, respectively. To a first-order
274 approximation $a_w = RH/100$. Aerosol volume growth is related via κ and RH by defining $f_v(RH)$
275 as the humidity-dependent ratio of wet and dry aerosol volume:

$$f_v(RH) \equiv \frac{V_{tot}}{V_d} = \frac{V_d + V_w}{V_d} = a + \kappa_v \frac{RH}{100 - RH} \qquad\qquad \text{Eq. 5}$$

276 Combining the previous equations and relating to a diameter D growth factor ($GF \equiv D/D_d$) yields

$$GF = \left(a + \kappa_v \frac{RH}{100 - RH} \right)^{1/3} \qquad\qquad \text{Eq. 6}$$

277 where $a = 1$, except for sea salt as discussed in Sect. 3.1. Reliable estimates of κ_v are available
278 for individual components (c.f. Table 2).
279
280   The next sections outline how we apply κ to represent mass and volume hygroscopic growth
281 in major hygroscopic aerosol components. Four components directly contribute to water uptake:
282 ammonium nitrate (ANO_3), ammoniated sulfate (ASO_4), sea salt (SS), and organics. We treat
283 black carbon (EBC), crustal material (CM), and trace oxides (TEO) as non-hygroscopic. We
284 evaluated inorganic component growth curves using the AIM model (Wexler and Clegg, 2002)
285 for RH = 10 – 90% except for sea salt, which included RH = 0%. Hygroscopic parameters were
286 matched to modeled fits. Aerosols are treated as internally mixed, without deliquescence or
287 efflorescence points, as discussed further below.

4.1. Inorganic behavior

289   Figure 1 shows the hygroscopic growth for inorganics. The κ_v value of 0.51 for ASO_4
290 best matches the AIM model over RH = 10-90% and is similar to the GF-derived $\kappa_v = 0.53$
291 estimated by Petters and Kreidenweis (2007). Our AIM-derived ANO_3 growth curve is smaller
292 than ASO_4, at $\kappa_v = 0.41$. Although both ammonium compounds share the same $GF = 1.6$ at RH =
293 85% (Sorooshian et al., 2008), ANO_3 is less hygroscopic at lower RH.
294
295   Sea salt accounts for a small fraction of aerosol mass over land, however its hydrophilic
296 nature makes it significant for water retention. A 1:1 volume ratio with water as RH approaches
297 0% (Kreidenweis et al., 2008) yields $a = 2$ (Eq. 2 and 3). A hygroscopic constant $\kappa_v = 1.5$ then
298 best fits AIM from the deliquescence point up to 90% RH.
299

300   We follow the widely used convention (e.g. Pitchford et al. (2007)) that $PM_{2.5}$ under
301   variable sub-saturated RH does not exhibit deliquescent phase transitions. There is compelling
302   evidence to adopt smooth hygroscopic growth curves. Various experiments show sub-
303   micrometer, internally mixed aerosols will not deliquesce as readily as pure compounds. For
304   example, Badger et al. (2006) observed ASO_4 aerosol deliquescence is clearly inhibited by the
305   presence of humic acids. A smooth growth curve has been observed over the range RH = 10 –
306   85% for ambient aerosols at Jungfraujoch (Swietlicki et al., 2008). Analysis of submicron aerosol
307   mixtures consisting of SS, ASO_4, ANO_3, and levoglucosan also showed no apparent phase
308   transition (Svenningsson et al., 2006).

309   ### 4.2. Organic matter behavior

310   Identifying a representative organic hygroscopic parameter is challenging, as many volume
311   growth curves are available based on a variety of laboratory experiments and field campaigns.
312   Organic composition varies by site, and by season. The Appendix table Al contains a collection
313   of hygroscopic parameters from the literature. Values for $\kappa_{v,OM}$ range from 0 to 0.2. We choose a
314   single $\kappa_{v,OM}$ value based on the oxygen/carbon ratio (O:C), which is a function of oxidation,
315   hence age of the organics. Generally O:C ratios are between 0.2 – 0.8 in urban environments
316   (Rickards et al., 2013). We select an O:C ratio of 0.5 to represent the populated nature of
317   SPARTAN sites (e.g. Robinson et al., 2013). This corresponds to an organic parameter of
318    $\kappa_{v,OM} = 0.1$ for a variety of organic mixtures (Jimenez et al., 2009).

319   ### 4.3. Aerosol water in multi-component systems

320   Mass-based hygroscopic water uptake κ_m is more convenient than κ_v to estimate water
321   retention in gravimetric analysis. The parameters κ_v and κ_m are related by water-normalized
322   density, $\kappa_{m,X} = \kappa_{v,X}/\rho_X$. Table 2 contains κ_v values identified for major aerosol chemical
323   components and densities. For a multi-component system we estimate aerosol water mass using a
324   mass-weighted combination of κ_m values:

$$\kappa_{m,tot} = \frac{1}{M}\sum_X m_X \kappa_{m,X} \qquad \text{Eq. 7}$$

325   Mass calculations are used to determine residual aerosol mass as described in Sect 4.9.
326   Estimates of total water uptake by volume are applied to aerosol light scatter in Sect. 5. The
327   volume parameter $\kappa_{v,tot}$ is similarly determined by a linear combination of volume-weighted
328   components X (e.g. Bezantakos et al., 2013):

$$\kappa_{v,tot} = \frac{1}{V}\sum_X v_X \kappa_{v,X} \qquad \text{Eq. 8}$$

329   The hygroscopic growth of ASO_4 and organic mixtures are treated as linear combinations of pure
330   compounds (Robinson et al., 2013). Errors in aerosol water uptake are less significant in mixtures
331   than for individual species due to dilution effects (Kreidenweis et al., 2008). For ambient aerosols,
332   empirically measured $\kappa_{v,tot}$ usually lies between 0.14 and 0.39 (Carrico et al., 2010).
333

4.4. Sources of Uncertainty

Uncertainty in atmospheric $PM_{2.5}$ concentrations can be separated into air volume and $PM_{2.5}$ mass. We estimated total flow volume variance to be ± 10%, while 2σ pre and post gravimetric mass measurement varied by a combined ± 4 μg. Characterization of hourly $PM_{2.5}$ uncertainties can be found in Appendix A2.

Of concern is the loss of semivolatiles after sampling. In the laboratory semivolatile loss is inhibited by storing filters in closed containers. As discussed in Section 2, the sampling protocol is designed to minimize semi-volatile loss. We tested the retention of semivolatile material in the field by examining the trend in $PM_{2.5}$ and ANO_3 mass from the first filter sampled (54 day residence time in instrument) through the last filter sampled (negligible residence time in instrument). Statistically insignificant trends were found for both $PM_{2.5}$ (-0.09 ± 0.46 μg m^{-3}/position) and ANO_3 (0.06 ± 0.15 μg m^{-3}/position) providing confidence in retention of semivolatiles on filters in the cartridge.

Other uncertainties include absolute equivalent black carbon mass due to the reflectivity path p (± 30%) and absorption cross section σ (± 30%), which combine to in quadrature ± 42%. Trace metal recovery yields were tested using a sequential second digestion with 20% nitric acid. Each acid-digested element was quantified by five dilutions of a 25 element standard (25 – 500 *ppb*) plus three internal calibration metals (Sc, In, Tb). The elemental comparison of crustal materials varies regionally (Wang, 2015), which contributes to CM uncertainty of ± 30% based on Al, Fe and Mg composition. Recovery of individual water-soluble elements was determined through 5-point anion and cation standards curves each with $r^2 > 98\%$ and <10% mass uncertainty for most elements at environmentally-relevant concentrations, including sulfate, nitrate, and ammonium. Based on lab filter spike tests, water-soluble ion extractions show > 95% extraction efficiency. Uncertainties of water-soluble ion yields are generally ± 5%, except when close to limit of detection (approximately 0.1 μg m^{-3}, depending on filter sampling duration). Errors in the component values affect our estimate of κ_v, which will affect the inferred aerosol water. Network evaluation is ongoing task that will continue over time.

5. Mass speciation results

5.1. Overview of $PM_{2.5}$ mass speciation

Gravimetrically-weighed $PM_{2.5}$ concentrations within the period June 2013 to February 2016 span an order of magnitude, from under 10 μg m^{-3} (e.g. Atlanta) to almost 100 μg m^{-3} (Kanpur). Sites include a variety of geographic regions including partial desert (Ilorin, Rehovot, Kanpur), coastline (Buenos Aires, Singapore), and developing megacities (Dhaka). Table 3 and Figure 2 contain the resulting $PM_{2.5}$ mass, composition, and location of each SPARTAN site. The mean SPARTAN composition over all sampling sites in descending concentration is 40% RM (primarily organic), 20% ASO_4, 13% CM, 12% EBC, 4.7% ANO_3, 2.3% SS and 1.0% TEO.

There is significant variation of relative and absolute speciation from these long-term averages. ASO_4 concentrations range from 1 μg m^{-3} (Buenos Aires, summer) to 17 μg m^{-3} (Kanpur, dry season). The fraction of sulfate in $PM_{2.5}$ exhibits much weaker spatial variation (10-

377   30%) as increases in ASO_4 coincide with increases in total $PM_{2.5}$. Hence locations with enhanced
378   sulfate tend to have enhancements in other aerosol components.
379
380   ANO_3 concentrations exhibit a larger spatial heterogeneity than sulfate. Absolute values
381   range over 30-fold, from 0.2 μg m^{-3} (Mammoth Cave, summer) to 6.8 μg m^{-3} (Kanpur, dry
382   season). Corresponding mass fractions are 7-8 % in Kanpur, Beijing, and Buenos Aires, and
383   below 2% in Bandung. This heterogeneity reflects large spatial and temporal variation in NH_3
384   and NO_x ($NO + NO_2$) sources. There were noticeable seasonal increases in ANO_3 during
385   wintertime periods in Beijing, Kanpur, and Dhaka, coinciding with lower temperatures.
386
387   CM concentrations span an order of magnitude from 1.0 μg m^{-3} (Atlanta) to 16 μg m^{-3}
388   (Beijing). The fraction of CM in $PM_{2.5}$ exhibits pronounced variation (5-25%). Except during
389   dust storms, CM does not show clear patterns of temporal or regional variation. This could be
390   explained by non-seasonal road dust, which may account for over 80% of CM in regions with
391   heavy urban traffic (Huang et al., 2015).
392
393   We used Zn:Al ratios to assess the relative importance of local road dust (*c.f.* Table 3).
394   Aluminum is mostly natural in origin (Zhang et al., 2006) whereas Zn is primarily from tire wear
395   (Begum et al., 2010; Councell et al., 2004). For example, ratios are above 3 for Dhaka and
396   Hanoi, but less than 0.3 for Mammoth Cave and South Dekalb site (Atlanta). In fine-mode
397   aerosols, the ratio tends to be highest in large cities distant from natural CM. In coarse-mode
398   aerosols, a low Zn:Al ratio (< 0.1) indicates the aerosol CM component is dominated by regional
399   dust.
400
401   Absolute EBC spans an eight-fold concentration range from 1.1 μg m^{-3} (Atlanta) to above 8
402   μg m^{-3} (Dhaka and Kanpur). Mass fractions of EBC ranged from 4% (Singapore) to 25%
403   (Manila). Trace element oxide (TEO) material is mainly composed of Zn, Pb, Ni, Cu, and Ba,
404   hence also derived mainly from anthropogenic sources. TEO contributes negligibly to total mass
405   (1%), as expected. Sea salt remains a consistently small contributor (2%) to total mass, except
406   for Buenos Aires and Rehovot (5-6%) due to coastal winds. Particle-bound water (PBW) mass at
407   35% humidity is determined from the growth parameter κ_m. PBW mass contribution is similar to
408   EBC (7%). At low humidity, the combined mass of ANO_3, EBC, TEO, sea salt, and PBW
409   account for 15-35 % of aerosol mass.
410
411   RM as inferred from mass reconstruction of inorganic compounds, PBW, and total filter-
412   weighed mass is implicitly treated as the organic aerosol mass fraction. In terms of relative
413   composition, RM spans a factor of two, from 30% mass in Buenos Aires to almost 60% in
414   Kanpur. Temporal changes in RM tend to coincide with increases in ASO_4, with an all-site $r^2 =$
415   0.92. Although RM is not fully independent of ASO_4, this relationship implies related sources.
416
417   We interpret the abundance of water-soluble potassium K relative to Al as an indicator of
418   wood smoke (e.g. Munchak et al., 2011). K:Al ratios averaged over each site range from < 2
419   (Mammoth Cave, Atlanta) to 16 (Kanpur), where combustion activity is apparent. Singapore was
420   downwind of significant Indonesian forest fire smoke during its sampling period of Aug-Nov
421   2015, averaging to K:Al = 13. The correlation between K:Al and RM across all SPARTAN sites
422   is $r^2 = 0.73$, supporting the attribution of RM as mostly organic.

423

424   Across all sites, coarse and fine mode mass fractions are approximately equal (0.50), with
425   fractions ranging from below 0.40 (Hanoi, Buenos Aires, and Manila) to above 0.55 (e.g.
426   Bandung, Kanpur, Atlanta, Mammoth Cave). The two size modes can be temporally correlated
427   per site, though sometimes weakly, from $r^2 = 0.15$ (Hanoi) to $r^2 = 0.76$ (Rehovot). We observe
428   strong temporal correlations between sulfate and ammonium in $PM_{2.5}$ ($r^2 = 0.72$ - 0.99). Nitrate
429   and ammonium are less consistently related (Table 3), ranging from higher values in Singapore
430   ($r^2 = 0.66$), Kanpur ($r^2 = 0.58$), Beijing ($r^2 = 0.28$), to weaker values in Ilorin and Manila ($r^2 <$
431   0.1). The strength of correlations with ammonium could be influenced by excess ammonium
432   relative to sulfate. The $[NH_4^+]/[SO_4^{2-}]$ ratio in $PM_{2.5}$ is 2.6 in Kanpur and 1.3 in Ilorin.

433   5.2. Collocation overview

434   We compare SPARTAN $PM_{2.5}$ speciation with previous studies available from the literature
435   and focus on collocated relative $PM_{2.5}$ composition of major components within the last 10 years.
436   TEO is omitted due to lack of significant mass contribution. Aerosol water content is also
437   omitted as it was not directly measured in any of the collocation studies. If not provided, CM is
438   treated as defined in Sect 4.5 where possible. Organic mass (OM) to organic carbon (OC) ratios
439   are from Philip et al. (2014b) with updates from Canagaratna et al. (2015).

440

441   Figure 3 provides an overview of the comparison studies organized by SPARTAN data
442   availability. Only sampling at Mammoth Cave sampling was temporally coincident with the
443   comparison data. SPARTAN compositional information is generally consistent with previous
444   studies, considering inter-annual chemical variation and measurement uncertainty. For example,
445   both SPARTAN and comparative studies find that $PM_{2.5}$ is composed of between 10-30% ASO_4
446   and 5-20% CM for sampled sites. SPARTAN EBC mass fraction generally matches within 5
447   percentage points of collocated studies, except for Bandung and Kanpur. SPARTAN and prior
448   studies find that ANO_3 is usually a small fraction of total mass, except at Beijing and Kanpur (7-
449   8%) due to their high agricultural and industrial activity. All studies find that sea-salt is below
450   3% of total mass. SPARTAN-derived RM has potentially the largest potential error, yet typically
451   is consistent with the combined organic and unknown masses of other studies. This offers further
452   evidence that SPARTAN measurements of RM are predominantly organic in nature.

453

454   5.3. Individual site characteristics

455   Below we discuss each site in more detail. We also examine how our chemical composition
456   from a global array of sites relate to local anthropogenic activities and surrounding area.
457   References to land type at specific sites are derived from Latham et al. (2014), unless otherwise
458   indicated. The number of filters is given in parentheses.

459

460   *5.3.1 Beijing, China (n = 114)*
461   Beijing has attracted considerable attention for its air pollution (Chen et al., 2013).
462 Agricultural areas to the west and the Gobi Desert to the north surround the city's 19 million
463 dwellers. The SPARTAN air sampler is located on the Tsinghua University campus, 15 km
464 northwest of the downtown center. This is our longest-running site, with 2.5 years of near-
465 continuous sampling. It reports the third-highest $PM_{2.5}$, at 69 μg m^{-3}, the third highest ASO_4 (12
466 μg m^{-3}) and the highest CM (16 μg m^{-3}) of all sites. The significant ANO_3 (5.5 μg m^{-3}) reflects

467 significant urban NO_x near agricultural NH_3 sources. ANO_3 values were highest during winter,
468 as expected from ammonium-nitrate thermodynamics. A high CM component in the springtime
469 reflects regional, natural CM sources. The mean $PM_{2.5}$ Zn:Al ratio is lower than other large cities
470 (0.51) likely due to larger fraction of natural dust sources and the sampling location in the
471 northwest quadrant of the city, upwind of many traffic sources. The lowest coarse-mode Zn:Al
472 mass ratios are observed in April 2014 (0.07) and April 2015 (0.06) during the annual Yellow
473 dust storm season. This is balanced by urban dust sources throughout the year, in agreement with
474 Lin et al. (2015) who found evidence of high CM in industrial areas of Beijing.

476 *Beijing Comparison:* Relative masses in Beijing compare well with previous studies.
477 SPARTAN ASO_4 (19%) is close to Yang et al. (2011) (17%) and Oanh et al. (2006) (20%)
478 and the RM of 37% is similar to combined OM (33 and 29%) and unknown fractions (10 and
479 24%) of comparison studies. SPARTAN ANO_3 concentrations (8.5%) are relatively higher
480 than most other locations, though lower than either previous study (11-12%), possibly due to
481 different sampling periods. CM is greater than Yang et al. (2011) (25% vs. 19%), and
482 significantly higher than Oanh et al. (2006) (5%), potentially due to a difference in
483 definitions.

485 ***5.3.2 Bandung, Indonesia (n = 77)***
486 Bandung is located inland on western Java surrounded by a volcanic mountain range and
487 agriculture (e.g. tea plantations). The sampler is located on the Institute of Technology Bandung
488 campus, 5 km north of the city center. Almost two years of sampling have resulted in a mean
489 $PM_{2.5}$ concentration of 31 µg m^{-3}. Sea salt is low at this elevated (826 m) inland site. ANO_3 and
490 CM levels are also low, but RM is moderately high compared with other sites, at 55%. This
491 could be explained by large amounts of vegetative burning; organic $PM_{2.5}$ mass fractions can rise
492 above 70% during combustion episodes (Fujii et al., 2014). Volcanic sources of sulfur, in
493 addition to industrial sources, may explain the relatively higher ASO_4 compared with Manila or
494 Dhaka (Lestari and Mauliadi, 2009). Influxes of volcanic dust from the Sinabang volcano from
495 August – September 2014 (2000 km northwest of Bandung) could explain why coarse-mode
496 Zn:Al ratios drop to 0.09 for this period compared to the annual mean of 0.21.

498 *Bandung Collocation:* Bandung is a volcanically active area, so that composition, in
499 particular ASO_4, differs due to naturally variable circumstances. SPARTAN ASO_4 (21%) is
500 higher than the 4% fraction reported by Lestari and Mauliadi (2009), but is identical with
501 measurements by Oanh et al. (2006). SPARTAN EBC (13%) is less than either previous
502 study (19% and 25%) and the more recent analysis of 19% BC (Santoso et al., 2013).
503 SPARTAN ANO_3 is 2% by mass, lower than measured by Oanh et al. (2006) (13%) but
504 similar to Lestari and Mauliadi (2009). Both of the earlier studies show lower RM fractions
505 (36%, and 42%) compared with 54% RM in this study.

507 ***5.3.3 Manila, Philippines (n = 63)***
508 Manila is a coastal city located in Manila Bay, adjacent to the South China Sea and
509 surrounded by mountains. The sampling station, located at the Manila Observatory, is about 40
510 m higher in altitude than the central city. The $PM_{2.5}$ concentrations at the observatory (18 µg m^{-3})
511 are expected to be lower than in the main city, but still influenced by vehicular traffic, fuel
512 combustion and industry (Cohen et al., 2009). Compared to the all-site average, the CM fraction

513 in Manila is typical (11%), but black carbon is twice as great (25%). The high EBC agrees with
514 previous observations, attributable to a relatively high use of diesel engines (Cohen et al., 2002).
515
516   *Manila Collocation:* SPARTAN fractions of ASO_4 and EBC are similar to Cohen et al.
517   (2009). Our RM (43%) is lower than OM (57%), whereas SPARTAN CM was greater than
518   Cohen et al. (2009). These differences could reflect sampling differences, or emission
519   changes over the last decade.
520
521   *5.3.4 Dhaka, Bangladesh (n = 41)*
522   Dhaka is a densely populated city (17,000 persons/km^2) in a densely populated country
523 (1,100 persons/km^2). The sampler is situated in the heart of downtown Dhaka, on the University
524 of Dhaka rooftop, and is influenced by air masses from the Indo Gangetic Plain (Begum et al.,
525 2012). More than half the country is used for agricultural purposes (Ahmed, 2013). Local
526 contributing $PM_{2.5}$ sources include coal and biomass burning, and heavy road traffic combustion
527 products and dust (Begum et al., 2010, 2012). $PM_{2.5}$ concentrations are the fourth highest of any
528 SPARTAN site, at 52 μg m^{-3}. Dhaka has the second-highest absolute EBC of any site, at 8.4 μg
529 m^{-3}, which can be explained by the abundance of truck diesel engines (Begum et al., 2012). We
530 estimate 41% of $PM_{2.5}$ in Dhaka is RM. Crop or bush burning on both local and regional scales
531 contribute significantly to organics (Begum et al., 2012). The high mean $PM_{2.5}$ Zn:Al ratio of 3.4
532 reflects a large contribution from urban traffic.
533
534   *5.3.5 Ilorin, Nigeria (n = 40)*
535   Ilorin is located in a rural area with low-level agriculture and shrub vegetation. The sampler
536 is sited on the university campus, 15 km east of the city of 500,000 people. Aerosol loadings
537 have seasonal cycles from agricultural burning events and dust storms (Generoso et al., 2003).
538 The RM accounted for two thirds of total $PM_{2.5}$ mass, among the largest, influenced by biomass
539 burning. There is evidence of biomass burning in the $PM_{2.5}$ peak in late spring 2014, and again in
540 2015. Lower ASO_4 (12%) compared to other SPARTAN sites reflects the sparse surrounding
541 industry. CM levels are comparable to other locations, except during dust storms. During a dust
542 storm (between April 14th - May 2nd 2015), CM increased to two thirds of $PM_{2.5}$ mass. The PM_c
543 Zn:Al ratio during the storm decreased to 0.01 versus 0.25 during non-storm days.
544
545   *5.3.6 Kanpur, India (n = 33)*
546   Kanpur is a city of 2.5 million people. The sampler is located at the IIT Kanpur campus
547 airstrip, about 10 km northwest of the city. The city lies in the Indo-Gangetic Plain, where
548 massive river floodplains are used for agricultural and industrial activity (Ram et al., 2012). We
549 sampled from December 2013 – May 2014, and September-November 2014, capturing one dry
550 season. SPARTAN-measured $PM_{2.5}$ for this period was 99 μg m^{-3}, the highest of any SPARTAN
551 site, of which 59% is RM, 19% ASO_4, and 7.4% ANO_3. The absolute values of all three
552 components are also the highest among those measured. Molar $[NH_4^+]:[SO_4^{2-}]$ ratios are higher
553 in Kanpur (2.6) than elsewhere. High background ammonia has been observed in the region
554 from satellite (e.g. Clarisse et al., 2009) which could explain the high levels of ANO_3. Wood
555 smoke is apparent from the high K:Al ratio (16), associated with organic matter burning during
556 winter dry months. We detected significant Zn concentrations (Zn:Al = 1.0), which is in
557 agreement with Misra et al. (2014) observations of a tripling of zinc during anthropogenic
558 sourced dust.

560 *Kanpur Collocation:* Relative fractions among the major species CM, salt, ASO_4 & ANO_3 all
561 match well with previous studies (Behera and Sharma, 2010; Chakraborty et al., 2015; Ram
562 et al., 2012) that also sampled during winter dry seasons. Chakraborty et al. (2015) measured
563 70% organic mass composition and found a combined mass of 28% for $ASO_4 + ANO_3$
564 compared to SPARTAN mass (26%). SPARTAN ASO_4 (19%) compares well to 13% of
565 Ram et al. (2012) and 18% for Behera and Sharma (2010), and ANO_3 (7.4%) is close to
566 previous values (6.1% and 6.6%). By comparison SPARTAN slightly overestimates EBC by
567 4-6%. SPARTAN CM (4.8%) is lower than Behera and Sharma (2010) (10%). Notably the
568 combined OM + unknown fractions from these previous two studies account for two thirds of
569 aerosol mass, 58% for Behera and Sharma (2010) and 63% for Ram et al. (2012), similar to
570 our 59% RM estimate. SPARTAN $PM_{2.5}$ concentrations, as well as RM, reach a maximum
571 during the month of December. This is consistent with recent work (Villalobos et al., 2015),
572 who attribute this increase to agricultural burning and stagnant air.

573

574 ### 5.3.7 Buenos Aires, Argentina (n = 31)
575 Buenos Aires has a metropolitan population of 12 million. SPARTAN instruments are
576 located on the urban CITEDEF campus 20 km west of the central downtown. The megacity, the
577 southernmost in our study, is surrounded by grassland and farming on the west and the Atlantic
578 Ocean on the east. The latter explains the relatively high proportion (6%) of sea salt. Total $PM_{2.5}$
579 (10 μg m^{-3}) and relative RM (31%) are low compared with other large metropolitan areas, likely
580 influenced by clean maritime air. In addition to sea salt and natural CM, the contribution of EBC
581 is 17%, which could reflect significant local truck diesel combustion (Jasan et al., 2009).

582

583 ### 5.3.8 Rehovot, Israel (n = 30)
584 Rehovot is located on a four-story rooftop on the Weizmann Institute campus, 11 km from
585 the Mediterranean Sea and 20 km south of Tel Aviv. The city is surrounded by semi-arid, mixed-
586 use cropland, and the region experiences occasional Saharan desert dust outbreaks. Typical $PM_{2.5}$
587 concentrations are low (16 μg m^{-3}), with the composition in Rehovot consisting of 29% ASO_4,
588 and 20% CM. The RM fraction is smaller in Rehovot (16% total $PM_{2.5}$ mass) than at other
589 SPARTAN sites. Aerosol sources in Israel include agriculture, desert dust, traffic and coal-based
590 power plants (Graham et al., 2004). Relative sodium concentrations are high in Rehovot (4%),
591 similar to Buenos Aires and Ilorin, and may include a contribution from dust.

592

593 *Lag Ba'Omer festival:* We measured high ASO_4 concentrations on May 7-18, 2015, during
594 which time a large number of bonfires were lit nearby. During the festival, over 75% of total
595 aerosol mass came from $ASO_4 + ANO_3$, leading to a brief doubling of the hygroscopic
596 parameter κ_v. We observed a K:Al ratio of 38 for May 6th of the festival, the highest for any
597 single filter.

598

599 *Saharan dust storm:* We had the opportunity to measure a severe dust storm in Rehovot from
600 a filter sampling February 4-13, 2015. The coarse filter Zn:Al ratio dropped to 0.02 during
601 the Saharan dust storm from the typical value of 0.3. On the coarse filter we obtained an
602 absolute CM mass of 950 μg, which accounts for half of the collected mass during the storm.
603 13% of dust storm PM_c is combined sea salt, ANO_3, and ASO_4, leaving 35% RM. Although

604   this RM fraction may imply an incomplete CM extraction, it is possible that a significant
605   portion of desert dust carries adsorbed organic material (Falkovich et al., 2004).
606
607   ### 5.3.9 Mammoth Cave NP, US (n = 19)
608   The Mammoth Cave sampling site straddles National Park mountainous terrain to the north
609   and east, with farmland to the south and west. It is about 35 km from the closest town, Bowling
610   Green, KY, with about 50,000 residents. Sources of PM are expected to be non-local, hence we
611   consider it our 'background' site.
612
613   *Mammoth Cave National Park Collocation*: This temporary SPARTAN site was deployed
614   for comparison with the IMPROVE network station (IMPROVE, 2015). Unique among our
615   sites, sampling was temporally coincident with IMPROVE's 1-in-3 day regimen. We
616   obtained quality-controlled samples from June-August 2014. Temporal variation in daily
617   values is consistent with IMPROVE for sulfate (r^2 = 0.86, slope = 1.03) and total mass of
618    $PM_{2.5}$ (r^2 = 0.76, slope = 1.12). Differences between IMPROVE vs. SPARTAN are small for
619   ASO_4 (36% vs. 33%), ANO_3 (2.4% vs. 1.2%), CM (7% vs. 11%), and EBC (3.0% vs. 5.6%),
620   respectively. The combined OM + unknown + water fraction IMPROVE was 51%, similar to
621   the SPARTAN RM mass fraction of 49%.
622
623   ### 5.3.10 Atlanta, US (n = 13)
624   Atlanta represents a major urban area in a developed country. The temporary SPARTAN site
625   was located at the South Dekalb supersite 15 km east of downtown Atlanta. Air sampling was
626   performed for a 4-month period spanning winter to spring 2014. Over the past 10 years
627   significant decreases in $PM_{2.5}$ have been observed here and across the eastern United States
628   (Boys et al., 2014). The surrounding region is tree-covered or agricultural.
629
630   *Atlanta* (*South Dekalb*) *Collocation:* Co-sampled filters from the Atlanta CSN station
631   (USEPA, 2015) provide a comparison with the summer 2014 SPARTAN data. The EPA OM
632   fraction (43%) agrees well with the SPARTAN mean RM (48%). Crustal, SS, EBC and
633   ASO_4 are within 2% relative to total composition. SPARTAN component fractions in Atlanta
634   are also consistent with respect to Butler et al. (2003); components CM (12% vs. 10%),
635   ASO_4 (23% vs. 28%), ANO_3 (3.5% vs 4%) and RM and OM (48% vs 55%) closely match,
636   except for EBC (11% vs. 3%), perhaps reflecting different time periods.
637
638   ### 5.3.11 Singapore, Singapore (n = 12)
639   Singapore is a densely populated coastal city-state at 7,770 people/km^2. The sampler is
640   located on a rooftop at the National University of Singapore (NUS), near the center of the city.
641   Transportation is mixed-use, including taxis, rail, and bicycles, which may help explain the
642   relatively low EBC and CM of 3%. Despite this, the Zn:Al ratio remains high at 1.5, implying a
643   dominant traffic-based contribution to CM. SPARTAN instruments have observed significant
644   biomass burning downwind from Indonesia, causing an increase in absolute $PM_{2.5}$ from 32 in
645   August to 120 μg m^{-3} in September 2015, as well as an increase in RM from 44% to 62%. The
646   K:Al ratio steadily increased during this same period, from 7.2 (Jul 24 – Aug 2, 2015) to 17 – 24
647   (Aug 11 – Sept 25).
648
649

650 ***5.3.12 Hanoi, Vietnam (n = 10)***
651   Hanoi is an inland megacity surrounded by grassland and agriculture. The sampler itself is on
652 a building rooftop at the Vietnam Academy of Science, 5 km northwest of the city center.
653 Motorbikes are the main forms of transportation downtown and the primary source of mobile-
654 based $PM_{2.5}$ (Vu Van et al., 2013). In Hanoi, the $PM_{2.5}$ Zn:Al ratio was 3.7, also the highest of
655 any SPARTAN site, indicative of significant traffic and tire wear.
656
657   *Hanoi Comparison:* SPARTAN $PM_{2.5}$ composition is generally consistent with Cohen et
658   al.(2010). Slight differences are perhaps related to differences in sampling season and
659   location. SPARTAN sea salt fraction was larger (2.5% vs. 0.6%), but with a lower ASO_4
660   fraction (17%) compared with Cohen et al. (2010) (29%). Sulfate tends to be lower in the
661   spring-summer seasons, coinciding with our measurement period, which may explain the
662   discrepancy. SPARTAN EBC (10%) is close to the Cohen et al. (2010) value of 8%, whereas
663   SPARTAN RM (51%) and CM (16%) masses are slightly higher.
664
665 ***5.3.13 Pretoria, South Africa (n = 5)***
666   Pretoria is a high-altitude city (1300 m) surrounded by arid, low-intensity agriculture and
667 extensive grasslands. The SPARTAN sampler is located on a 10m CSIR building rooftop 12 km
668 east of downtown area (*pop.* 700,000). Preliminary measurements of south-hemisphere
669 springtime show absolute $PM_{2.5}$ concentrations to be low, at 6.4 µg m^{-3}. There are significant
670 fractions of CM (22%) and EBC (22%), and low RM (14%). The $PM_{2.5}$ Zn:Al ratio (0.69)
671 indicates vehicle traffic contributes to CM.

672 ## 6. Refining estimates of dry hourly $PM_{2.5}$ using κ_v

673 Our assessment of $PM_{2.5}$ hygroscopicity is determined by site-specific chemical composition. We
674 then use the time-varying hygroscopicity to refine the $PM_{2.5}$ values inferred from nephelometer
675 scatter.

676   ### 6.1. Relating $PM_{2.5}$ composition to κ_v

677   The outer pie charts of Figure 2 show the site-mean hygroscopic growth constant κ_v,
678 surrounded by the water contributions at 35% RH. The major contributors to PBW are ASO_4,
679 ANO_3, RM, and sea salt, as inferred from the values listed in Table 2 and weighted by
680 composition as in Eq. 5. ASO_4 and RM contribute similarly to total aerosol water whereas ANO_3
681 contributes less to $PM_{2.5}$ hygroscopicity due to its smaller mass. The contribution of sea salt to
682 hygroscopicity can be significant, and makes a dominant contribution in both Rehovot and
683 Buenos Aires.
684
685   The parameter κ_v, when averaged across all sites, is 0.20, matching the generic estimate
686 $\kappa_{v,tot} = 0.2$ applied in the initial SPARTAN study (Snider et al., 2015). Recently Brock et al.
687 (2016) estimate κ_v values between 0.15 and 0.25 for ambient aerosols with 50% orgnic
688 composition at subsaturated humidity. The local SPARTAN value in Atlanta (0.17) is consistent
689 the value of 0.16 ± 0.07 by Padró et al. (2012) in Atlanta. We found significant long-term
690 differences in $\kappa_{v,tot}$ between cities, from 0.15 in Ilorin to 0.28 in Rehovot, and differences
691 between filters at single sites (σ ∼ 0.05). There is little correlation of $\kappa_{v,tot}$ with changes in mass
692 ($r^2 < 0.01$). However, there are significant changes in $\kappa_{v,tot}$ due to seasonality and specific

693 events (e.g. dust storms, fires). In Beijing, aerosol hygroscopicity was 50% higher in mid
694 summer (August) due to increased sulfate, and in late winter (March) due to a relative increase in
695 sea salt. A summertime sulfate peak also agrees with observations by Yang et al. (2011). Table 3
696 shows the site-specific PBW in $PM_{2.5}$. At RH =35%, PBW ranges from $0.6 - 6$ µg m^{-3},
697 comparable in absolute values to EBC. Above 80% RH PBW will account for more than half of
698 aerosol mass. Accounting for this water component in nephelometer scatter motivates the
699 following section.

6.2. Relating nephelometer scatter to dry (RH=35%) $PM_{2.5}$

701 We apply a temporally resolved, site-specific κ_v to refine our relationship between total
702 nephelometer scatter and $PM_{2.5}$. We calculate a 45-day running mean aerosol volume-weighted
703 κ_v at each SPARTAN site. We then use the hygroscopic growth factors to estimate dry hourly
704 $PM_{2.5}$ from hourly nephelometer measurements of ambient scatter and hourly measured RH.
705 Appendix A2 describes the procedure in more detail.
706
707 We compared our hourly $PM_{2.5}$ in Beijing with $PM_{2.5}$ measurements from a Beta Attenuation
708 Monitor (MetOne) at the US Embassy, located 15 km away. The left panel of Figure 4 shows the
709 time series of hourly dry $PM_{2.5}$ concentrations predicted by SPARTAN during the summer.
710 Pronounced temporal variation is apparent, with $PM_{2.5}$ concentrations varying by more than an
711 order of magnitude. A high degree of consistency is found with the BAM ($r^2 = 0.67$). The
712 exclusion of water uptake in hourly $PM_{2.5}$ estimates (by setting all $\kappa_v = 0$) decreased hourly
713 correlations slightly to $r^2 = 0.62$. The average humidity in Beijing was 47% for the measurement
714 period, corresponding to a mean 17% volume contribution by water ($\kappa_v = 0.19$). Hygroscopic
715 growth should play a more significant role under more humid conditions (e.g. Manila and
716 Dhaka).
717
718 The right panel shows daily-averaged $PM_{2.5}$ ($n = 148$). In 2014 there were 3167
719 coincidentally available hours with which to compare. The coefficient of variation for averaged
720 24-hour measurements remained high ($r^2 = 0.70$). There was a mean offset of 10 µg m^{-3}.
721 However the slope is near unity (0.98), suggesting excellent proportionality between our
722 nephelometer and the BAM instrument for $PM_{2.5}$ concentrations below 200 µg m^{-3}. Above this
723 concentration, nephelometer signals become non-linear. The agreement remained similar for
724 hourly values ($r^2 = 0.67$).
725

7. Conclusions

727
728 We have established a multi-country network where continuous monitoring with a 3-
729 wavelength nephelometer is combined with a single multi-day composite filter sample to provide
730 information on $PM_{2.5}$. Long-term average aerosol composition is inferred from the filters,
731 including equivalent black carbon, sea salt, crustal material, ammoniated sulfate, and ammonium
732 nitrate. This composition information was applied to calculate aerosol hygroscopicity, and in turn
733 the relation between aerosol scatter at ambient and controlled RH. These data provide a
734 consistent set of compositional measurements from 13 sites in 11 countries.
735

736   We report ongoing measurements of fine particulate matter ($PM_{2.5}$), including compositional
737   information, in 13 locations in two month or greater intervals all within a three-year span (2013-
738   2016). The mean composition averaged for all SPARTAN sites is ammoniated sulfate (20% ±
739   11%), crustal material (13.4% ± 9.9%), black carbon (11.9% ± 8.4%), ammonium nitrate (4.7%
740   ± 3.0%), sea salt (2.3% ± 1.6%), trace element oxides (1.0% ± 1.1%), water (7.2% ± 3.3%) at
741   35% RH, and residual matter, which is probably primarily organic (40% ± 24%).
742
743   Analysis of filter samples reveals that several $PM_{2.5}$ chemical components varied by more
744   than an order of magnitude between sites. Ammoniated sulfate ranged from 1 μg m^{-3} in Buenos
745   Aires to 17 μg m^{-3} in Kanpur (dry season). Ammonium nitrate ranged from 0.2 μg m^{-3}
746   (Mammoth Cave, summertime) to 6.8 μg m^{-3} (Kanpur, dry season). Equivalent black carbon
747   ranged from 0.7 μg m^{-3} (Mammoth Cave) to 8 μg m^{-3} (Dhaka and Kanpur). Locations with
748   enhanced sulfate tend to have enhancements in other PM components. For example, ammoniated
749   sulfate and residual matter (probably organic) are highly correlated across sites ($r^2 = 0.92$).
750
751   Crustal material concentrations ranged from 1 μg m^{-3} (Atlanta) to 16 μg m^{-3} (Beijing).
752   Measuring Zn:Al ratios in $PM_{2.5}$ was an effective way to determine anthropogenic contribution
753   to crustal material. Ratios larger than 0.5 identified sites with significant road dust contributions
754   (e.g. in Hanoi, Dhaka, Manila, and Kanpur). Some locations, such as Beijing and Buenos Aires,
755   had both high anthropogenic and natural crustal material. Low coarse Zn:Al ratios were apparent
756   during natural dust storms. Anthropogenic crustal material is an aerosol component neglected by
757   most global models and which may deserve more attention.
758
759   Potassium is a known marker for wood smoke. Enhanced K:Al ratios were found in
760   Singapore downwind of Indonesian forest fires, in Kanpur during the winter dry season from
761   agricultural burning, and in Rehovot during a bonfire festival. Furthermore, these ratios were
762   correlated with RM concentrations ($r^2 = 0.73$), supporting the attribution of RM as mostly
763   organic.
764
765   SPARTAN measurements generally agree well with previous collocated studies. SPARTAN
766   sulfate fractions are within 4% of fractions measured at eight of the ten collocated, though
767   temporally non-coincident, studies. Dedicated contemporaneous collocation with IMPROVE at
768   Mammoth Cave yielded a high degree of consistency with daily sulfate ($r^2 = 0.86$, slope = 1.03),
769   daily $PM_{2.5}$ ($r^2 = 0.76$, slope = 1.12), and mean fractions for all major $PM_{2.5}$ components (within
770   2%). Crustal material is typically consistent with the previous measurements, at 5-15%
771   composition. SPARTAN equivalent black carbon ranged broadly, from 3% (Singapore) to 25%
772   (Manila), and matched within a few percent of most previous works. Ammonium nitrate (4%)
773   generally matched other sites, though it was sometimes lower, as in Beijing and Atlanta. Sea-salt
774   was consistently low, as found in previous measurements. Sea salt fractions were highest in
775   Buenos Aires and Rehovot (6%), reflecting natural coastal aerosols. SPARTAN residual matter
776   is consistent with the combined organic and unknown masses. Comparing with collocated
777   measurements supports the expectation that most of the RM is partially organic. Residual matter
778   could also include unaccounted-for particle bound water, measurement error, and possibly
779   unmeasured inorganic materials.
780

781  We calculated the hygroscopic constant κ_v for individual PM$_{2.5}$ filters to estimate water at
782 variable humidity, and to infer wet and water-free residual matter. Based on a range of literature,
783 we treated residual matter as mostly organic, with constant $\kappa_{v,RM} = 0.1$. Residual matter and
784 ammoniated sulfate largely determined overall water uptake in aerosols. These individual
785 species, along with sea salt and ammonium nitrate, resulted in a mean mixed hygroscopic
786 constant of 0.20, implying that for many sites, water content above 80% RH will account for
787 more than half of aerosol mass. For cleanroom conditions of low humidity (35% RH), mean
788 water composition was estimated to be 7% by mass.
789

790  Water retention calculations allow for volumetric fluctuation estimates of aerosol water at
791 variable RH. We subtracted the water component to predict dry nephelometer scatter as a
792 function of time, anchored to filter masses at 35% RH. For Beijing, we assessed the consistency
793 of SPARTAN predictions of hourly PM$_{2.5}$ values with BAM measurements taken 15 km away,
794 and found temporal consistency ($r^2 = 0.67$), with a slope near unity (0.98). The explained
795 variance decreased to $r^2 = 0.62$ when setting $\kappa_v = 0$. This comparison tested both SPARTAN
796 instrumentation and our treatment of aerosol water uptake.
797

798  These measurements provide chemical and physical data for future research on PM$_{2.5}$.
799 Collocation with sun photometer measurements of AOD connects satellite observations to
800 ground-based measurements and provides information needed to evaluate chemical transport
801 model simulations of the PM$_{2.5}$ to AOD ratio. As sampling expands, SPARTAN will provide
802 long-term data on fine aerosol variability from around the world. Ongoing work includes an
803 analysis of trace metal concentrations and interpreting SPARTAN measurements with a
804 chemical transport model. The data are freely available as a public good at www.spartan-
805 network.org. We welcome expressions of interest to join this grass-roots network.
806

Acknowledgements

807

808 SPARTAN is an IGAC-endorsed activity (www.igacproject.org). The Natural Sciences and
809 Engineering Research Council (NSERC) of Canada supported this work. We are grateful to
810 many who have offered helpful comments and advice on the creation of this network including
811 Jay Al-Saadi, Ross Anderson, Kalpana Balakrishnan, Len Barrie, Sundar Christopher, Matthew
812 Cooper, Jim Crawford, Doug Dockery, Jill Engel-Cox, Greg Evans, Markus Fiebig, Allan
813 Goldstein, Judy Guernsey, Ray Hoff, Rudy Husar, Mike Jerrett, Michaela Kendall, Rich
814 Kleidman, Petros Koutrakis, Glynis Lough, Doreen Neil, John Ogren, Norm O'Neil, Jeff Pierce,
815 Thomas Holzer-Popp, Ana Prados, Lorraine Remer, Sylvia Richardson, and Frank Speizer. Data
816 collection Rehovot was supported in part by the Environmental Health Fund (Israel) and the
817 Weizmann Institute. Partial support for the ITB site was under the grant HIBAH WCU-ITB. The
818 site at IIT Kanpur is supported in part by National Academy of Sciences and USAID. The views
819 expressed here are of authors and do not necessarily reflect those of NAS or USAID. The
820 Singapore site is supported by the Singapore National Research Foundation (NRF) through the
821 Singapore-MIT Alliance for Research and Technology (SMART), Center for Environmental
822 Sensing and Modeling.

823

8. References

Ahmed, S.: Food and Agriculture in Bangladesh, Encycl. Food Agric. Ethics, doi:10.1007/978-94-007-6167-4_61-2, 2013.

Asa-Awuku, A., Moore, R. H., Nenes, A., Bahreini, R., Holloway, J. S., Brock, C. A., Middlebrook, A. M., Ryerson, T. B., Jimenez, J. L., DeCarlo, P. F., Hecobian, A., Weber, R. J., Stickel, R., Tanner, D. J., and Huey, L. G.: Airborne cloud condensation nuclei measurements during the 2006 Texas Air Quality Study, J. Geophys. Res. Atmos., 116(D11), D11201, doi:10.1029/2010JD014874, 2011.

Badger, C. L., George, I., Griffiths, P. T., Braban, C. F., Cox, R. A., and Abbatt, J. P. D.: Phase transitions and hygroscopic growth of aerosol particles containing humic acid and mixtures of humic acid and ammonium sulphate, Atmos. Chem. Phys., 6(3), 755–768, doi:10.5194/acp-6-755-2006, 2006.

Barnard, J. C., Volkamer, R., and Kassianov, E. I.: Estimation of the mass absorption cross section of the organic carbon component of aerosols in the Mexico City Metropolitan Area, Atmos. Chem. Phys., 8(22), 6665–6679, doi:10.5194/acp-8-6665-2008, 2008.

Begum, B. A., Biswas, S. K., Markwitz, A., and Hopke, P. K.: Identification of sources of fine and coarse particulate matter in Dhaka, Bangladesh, Aerosol Air Qual. Res., 10, 345–353, doi:10.4209/aaqr.2009.12.0082, 2010.

Begum, B. A., Hossain, A., Nahar, N., Markwitz, A., and Hopke, P. K.: Organic and Black Carbon in PM2.5 at an Urban Site at Dhaka, Bangladesh, Aerosol Air Qual. Res., 12(6), 1062–1072, 2012.

Behera, S. N., and Sharma, M.: Reconstructing Primary and Secondary Components of PM2.5 Composition for an Urban Atmosphere, Aerosol Sci. Technol., 44(11), 983–992, doi:10.1080/02786826.2010.504245, 2010.

Bell, M. L., Dominici, F., Ebisu, K., Zeger, S. L., and Samet, J. M.: Spatial and Temporal Variation in PM2.5 Chemical Composition in the United States for Health Effects Studies, Environ. Health Perspect., 115(7), 989–995, doi:10.2307/4619499, 2007.

Bezantakos, S., Barmpounis, K., Giamarelou, M., Bossioli, E., Tombrou, M., Mihalopoulos, N., Eleftheriadis, K., Kalogiros, J., D. Allan, J., Bacak, A., Percival, C. J., Coe, H., and Biskos, G.: Chemical composition and hygroscopic properties of aerosol particles over the Aegean Sea, Atmos. Chem. Phys., 13(22), 11595–11608, doi:10.5194/acp-13-11595-2013, 2013.

Bond, T. C. and Bergstrom, R. W.: Light Absorption by Carbonaceous Particles: An Investigative Review, Aerosol Sci. Technol., 40(1), 27–67, doi:10.1080/02786820500421521, 2006.

Boys, B. L., Martin, R. V, van Donkelaar, A., MacDonell, R. J., Hsu, N. C., Cooper, M. J., Yantosca, R. M., Lu, Z., Streets, D. G., Zhang, Q., and Wang, S. W.: Fifteen-Year Global Time Series of Satellite-Derived Fine Particulate Matter, Environ. Sci. Technol., 48(19), 11109–11118, doi:10.1021/es502113p, 2014.

Brauer, M., Freedman, G., Frostad, J., van Donkelaar, A., Martin, R. V, Dentener, F., Dingenen, R. van, Estep, K., Amini, H., Apte, J. S., Balakrishnan, K., Barregard, L., Broday, D., Feigin, V., Ghosh, S., Hopke, P. K., Knibbs, L. D., Kokubo, Y., Liu, Y., Ma, S., Morawska, L., Sangrador, J. L. T., Shaddick, G., Anderson, H. R., Vos, T., Forouzanfar, M. H., Burnett, R. T., and Cohen, A.: Ambient Air Pollution Exposure Estimation for the Global Burden of Disease 2013, Environ. Sci. Technol., doi:10.1021/acs.est.5b03709, 2015.

Brock, C. A., Wagner, N. L., Anderson, B. E., Attwood, A. R., Beyersdorf, A., Campuzano-Jost, P., Carlton, A. G., Day, D. A., Diskin, G. S., Gordon, T. D., Jimenez, J. L., Lack, D. A., Liao, J., Markovic, M. Z., Middlebrook, A. M., Ng, N. L., Perring, A. E., Richardson, M. S., Schwarz, J. P., Washenfelder, R. A., Welti, A., Xu, L., Ziemba, L. D., and Murphy, D. M.: Aerosol optical properties in the southeastern United States in summer – Part 1: Hygroscopic growth, Atmos. Chem. Phys., 16(8), 4987–5007, doi:10.5194/acp-16-4987-2016, 2016.

Butler, A. J., Andrew, M. S., and Russell, A. G.: Daily sampling of PM2.5 in Atlanta: Results of the first year of the Assessment of Spatial Aerosol Composition in Atlanta study, J. Geophys. Res. Atmos., 108(D7), 8415, doi:10.1029/2002JD002234, 2003.

Canagaratna, M. R., Jimenez, J. L., Kroll, J. H., Chen, Q., Kessler, S. H., Massoli, P., Hildebrandt Ruiz, L., Fortner, E., Williams, L. R., Wilson, K. R., Surratt, J. D., Donahue, N. M., Jayne, J. T., and Worsnop, D. R.: Elemental ratio

871   measurements of organic compounds using aerosol mass spectrometry: characterization, improved calibration, and
872   implications, Atmos. Chem. Phys., 15(1), 253–272, doi:10.5194/acp-15-253-2015, 2015.

873   Carrico, C. M., Petters, M. D., Kreidenweis, S. M., Sullivan, A. P., McMeeking, G. R., Levin, E. J. T., Engling, G.,
874   Malm, W. C., and Collett, J. L.: Water uptake and chemical composition of fresh aerosols generated in open burning
875   of biomass, Atmos. Chem. Phys., 10(11), 5165–5178, doi:10.5194/acp-10-5165-2010, 2010.

876   Chakraborty, A., Bhattu, D., Gupta, T., Tripathi, S. N., and Canagaratna, M. R.: Real-time measurements of ambient
877   aerosols in a polluted Indian city: Sources, characteristics, and processing of organic aerosols during foggy and
878   nonfoggy periods, J. Geophys. Res. Atmos., 120(17), 2015JD023419, doi:10.1002/2015JD023419, 2015.

879   Chang, R. Y.-W., Slowik, J. G., Shantz, N. C., Vlasenko, A., Liggio, J., Sjostedt, S. J., Leaitch, W. R., and Abbatt, J.
880   P. D.: The hygroscopicity parameter (κ) of ambient organic aerosol at a field site subject to biogenic and
881   anthropogenic influences: relationship to degree of aerosol oxidation, Atmos. Chem. Phys., 10(11), 5047–5064,
882   doi:10.5194/acp-10-5047-2010, 2010.

883   Chen, H., Goldberg, M. S., and Villeneuve, P. J.: A systematic review of the relation between long-term exposure to
884   ambient air pollution and chronic diseases., Rev. Environ. Health, 23(4), 243–297, 2008.

885   Chen, Z., Wang, J.-N., Ma, G.-X., and Zhang, Y.-S.: China tackles the health effects of air pollution, Lancet,
886   382(9909), 1959–1960, 2013.

887   Chow, J. C., Watson, J. G., Park, K., Lowenthal, D. H., Robinson, N. F., and Magliano, K. A.: Comparison of
888   particle light scattering and fine particulate matter mass in central California., J. Air Waste Manage. Assoc., 56(4),
889   398–410, 2006.

890   Chu, S.-H.: PM2.5 episodes as observed in the speciation trends network, Atmos. Environ., 38(31), 5237–5246,
891   doi:10.1016/j.atmosenv.2004.01.055, 2004.

892   Clarisse, L., Clerbaux, C., Dentener, F., Hurtmans, D., and Coheur, P.-F.: Global ammonia distribution derived from
893   infrared satellite observations, Nat. Geosci, 2(7), 479–483, 2009.

894   Cohen, D. D., Garton, D., Stelcer, E., Wang, T., Poon, S., Kim, J., Oh, S. N., Shin, H.-J., Ko, M. Y., and Santos, F.:
895   Characterisation of PM2. 5 and PM10 fine particle pollution in several Asian regions., 2002.

896   Cohen, D. D., Stelcer, E., Santos, F. L., Prior, M., Thompson, C., and Pabroa, P. C. B.: Fingerprinting and source
897   apportionment of fine particle pollution in Manila by IBA and PMF techniques: A 7-year study, X-Ray Spectrom.,
898   38(1), 18–25, doi:10.1002/xrs.1112, 2009.

899   Cohen, D. D., Crawford, J., Stelcer, E., and Bac, V. T.: Characterisation and source apportionment of fine
900   particulate sources at Hanoi from 2001 to 2008, Atmos. Environ., 44(3), 320–328,
901   doi:10.1016/j.atmosenv.2009.10.037, 2010.

902   Councell, T. B., Duckenfield, K. U., Landa, E. R., and Callender, E.: Tire-Wear Particles as a Source of Zinc to the
903   Environment, Environ. Sci. Technol., 38(15), 4206–4214, doi:10.1021/es034631f, 2004.

904   Dabek-Zlotorzynska, E., Dann, T. F., Kalyani Martinelango, P., Celo, V., Brook, J. R., Mathieu, D., Ding, L., and
905   Austin, C. C.: Canadian National Air Pollution Surveillance (NAPS) PM2.5 speciation program: Methodology and
906   PM2.5 chemical composition for the years 2003–2008, Atmos. Environ., 45(3), 673–686, 2011.

907   van Donkelaar, A., Martin, R. V, Brauer, M., and Boys, B. L.: Use of Satellite Observations for Long-Term
908   Exposure Assessment of Global Concentrations of Fine Particulate Matter, Environ. Health Perspect., 123(2), 135–
909   143, doi:10.1289/ehp.1408646, 2015.

910   Duplissy, J., DeCarlo, P. F., Dommen, J., Alfarra, M. R., Metzger, A., Barmpadimos, I., Prevot, A. S. H.,
911   Weingartner, E., Tritscher, T., Gysel, M., Aiken, A. C., Jimenez, J. L., Canagaratna, M. R., Worsnop, D. R., Collins,
912   D. R., Tomlinson, J., and Baltensperger, U.: Relating hygroscopicity and composition of organic aerosol particulate
913   matter, Atmos. Chem. Phys., 11(3), 1155–1165, doi:10.5194/acp-11-1155-2011, 2011.

914   Dusek, U., Frank, G. P., Massling, A., Zeromskiene, K., Iinuma, Y., Schmid, O., Helas, G., Hennig, T.,
915   Wiedensohler, A., and Andreae, M. O.: Water uptake by biomass burning aerosol at sub- and supersaturated
916   conditions: closure studies and implications for the role of organics, Atmos. Chem. Phys., 11(18), 9519–9532,

917   doi:10.5194/acp-11-9519-2011, 2011.

918   Falkovich, A. H., Schkolnik, G., Ganor, E., and Rudich, Y.: Adsorption of organic compounds pertinent to urban
919   environments onto mineral dust particles, J. Geophys. Res. Atmos., 109(D2), n/a–n/a, doi:10.1029/2003JD003919,
920   2004.

921   Fang, T., Guo, H., Verma, V., Peltier, R. E., and Weber, R. J.: $PM_{2.5}$ water-soluble elements in the southeastern
922   United States: automated analytical method development, spatiotemporal distributions, source apportionment, and
923   implications for heath studies, Atmos. Chem. Phys., 15(20), 11667–11682, doi:10.5194/acp-15-11667-2015, 2015.

924   Forouzanfar, M. H., Alexander, L., Anderson, H. R., Bachman, V. F., Biryukov, S., Brauer, M., Burnett, R., Casey,
925   D., Coates, M. M., Cohen, A., Delwiche, K., Estep, K., Frostad, J. J., KC, A., Kyu, H. H., Moradi-Lakeh, M., Ng,
926   M., Slepak, E. L., Thomas, B. A., Wagner, J., Aasvang, G. M., Abbafati, C., Ozgoren, A. A., Abd-Allah, F., Abera,
927   S. F., Aboyans, V., Abraham, B., Abraham, J. P., Abubakar, I., Abu-Rmeileh, N. M. E., Aburto, T. C., Achoki, T.,
928   Adelekan, A., Adofo, K., Adou, A. K., Adsuar, J. C., Afshin, A., Agardh, E. E., Al Khabouri, M. J., Al Lami, F. H.,
929   Alam, S. S., Alasfoor, D., Albittar, M. I., Alegretti, M. A., Aleman, A. V, Alemu, Z. A., Alfonso-Cristancho, R.,
930   Alhabib, S., Ali, R., Ali, M. K., Alla, F., Allebeck, P., Allen, P. J., Alsharif, U., Alvarez, E., Alvis-Guzman, N.,
931   Amankwaa, A. A., Amare, A. T., Ameh, E. A., Ameli, O., Amini, H., Ammar, W., Anderson, B. O., Antonio, C. A.
932   T., Anwari, P., Cunningham, S. A., Arnlöv, J., Arsenijevic, V. S. A., Artaman, A., Asghar, R. J., Assadi, R., Atkins,
933   L. S., Atkinson, C., Avila, M. A., Awuah, B., Badawi, A., Bahit, M. C., Bakfalouni, T., Balakrishnan, K., Balalla,
934   S., Balu, R. K., Banerjee, A., Barber, R. M., Barker-Collo, S. L., Barquera, S., Barregard, L., Barrero, L. H.,
935   Barrientos-Gutierrez, T., Basto-Abreu, A. C., Basu, A., Basu, S., Basulaiman, M. O., Ruvalcaba, C. B., Beardsley,
936   J., Bedi, N., Bekele, T., Bell, M. L., Benjet, C., Bennett, D. A., et al.: Global, regional, and national comparative risk
937   assessment of 79 behavioural, environmental and occupational, and metabolic risks or clusters of risks in 188
938   countries, 1990–2013: a systematic analysis for the Global Burden of Disease Study 2013, Lancet,
939   doi:10.1016/S0140-6736(15)00128-2, 2015.

940   Fountoukis, C. and Nenes, A.: ISORROPIA II: a computationally efficient thermodynamic equilibrium model for
941   aerosols, Atmos. Chem. Phys., 7(17), 4639–4659, doi:10.5194/acp-7-4639-2007, 2007.

942   Fujii, Y., Iriana, W., Oda, M., Puriwigati, A., Tohno, S., Lestari, P., Mizohata, A., and Huboyo, H. S.:
943   Characteristics of carbonaceous aerosols emitted from peatland fire in Riau, Sumatra, Indonesia, Atmos. Environ.,
944   87, 164–169, doi:10.1016/j.atmosenv.2014.01.037, 2014.

945   Generoso, S., Bréon, F.-M., Balkanski, Y., Boucher, O., and Schulz, M.: Improving the seasonal cycle and
946   interannual variations of biomass burning aerosol sources, Atmos. Chem. Phys., 3(4), 1211–1222, doi:10.5194/acp-
947   3-1211-2003, 2003.

948   Gibson, M. D., Heal, M. R., Bache, D. H., Hursthouse, A. S., Beverland, I. J., Craig, S. E., Clark, C. F., Jackson, M.
949   H., Guernsey, J. R., and Jones, C.: Using Mass Reconstruction along a Four-Site Transect as a Method to Interpret
950   PM10 in West-Central Scotland,United Kingdom, J. Air Waste Manage. Assoc., 59(12), 1429–1436,
951   doi:10.3155/1047-3289.59.12.1429, 2009.

952   Gibson, M. D., Pierce, J. R., Waugh, D., Kuchta, J. S., Chisholm, L., Duck, T. J., Hopper, J. T., Beauchamp, S.,
953   King, G. H., Franklin, J. E., Leaitch, W. R., Wheeler, A. J., Li, Z., Gagnon, G. A., and Palmer, P. I.: Identifying the
954   sources driving observed PM2.5 temporal variability over Halifax, Nova Scotia, during BORTAS-B, Atmos. Chem.
955   Phys., 13(14), 7199–7213, doi:10.5194/acp-13-7199-2013, 2013a.

956   Gibson, M. D., Heal, M. R., Li, Z., Kuchta, J., King, G. H., Hayes, A., and Lambert, S.: The spatial and seasonal
957   variation of nitrogen dioxide and sulfur dioxide in Cape Breton Highlands National Park, Canada, and the
958   association with lichen abundance, Atmos. Environ., 64(0), 303–311,
959   doi:http://dx.doi.org/10.1016/j.atmosenv.2012.09.068, 2013b.

960   Giordano, M. R., Short, D. Z., Hosseini, S., Lichtenberg, W., and Asa-Awuku, A. A.: Changes in Droplet Surface
961   Tension Affect the Observed Hygroscopicity of Photochemically Aged Biomass Burning Aerosol, Environ. Sci.
962   Technol., 47(19), 10980–10986, doi:10.1021/es401867j, 2013.

963   Graham, B., Falkovich, A. H., Rudich, Y., Maenhaut, W., Guyon, P., and Andreae, M. O.: Local and regional
964   contributions to the atmospheric aerosol over Tel Aviv, Israel: a case study using elemental, ionic and organic
965   tracers, Atmos. Environ., 38(11), 1593–1604, doi:http://dx.doi.org/10.1016/j.atmosenv.2003.12.015, 2004.

966 Hand, J. and Malm, W. C.: Review of the IMPROVE Equation for Estimating Ambient Light Extinction
967 Coefficients, Colorado State University, Fort Colins., 2006.

968 Hand, J. L., Schichtel, B. A., Pitchford, M., Malm, W. C., and Frank, N. H.: Seasonal composition of remote and
969 urban fine particulate matter in the United States, J. Geophys. Res., 117(D5), D05209, doi:10.1029/2011JD017122,
970 2012.

971 Henning, S., Weingartner, E., Schwikowski, M., Gäggeler, H. W., Gehrig, R., Hinz, K.-P., Trimborn, A., Spengler,
972 B., and Baltensperger, U.: Seasonal variation of water-soluble ions of the aerosol at the high-alpine site Jungfraujoch
973 (3580 m asl), J. Geophys. Res. Atmos., 108(D1), 4030, doi:10.1029/2002JD002439, 2003.

974 Hersey, S. P., Craven, J. S., Metcalf, A. R., Lin, J., Lathem, T., Suski, K. J., Cahill, J. F., Duong, H. T., Sorooshian,
975 A., Jonsson, H. H., Shiraiwa, M., Zuend, A., Nenes, A., Prather, K. A., Flagan, R. C., and Seinfeld, J. H.:
976 Composition and hygroscopicity of the Los Angeles Aerosol: CalNex, J. Geophys. Res. Atmos., 118(7), 3016–3036,
977 doi:10.1002/jgrd.50307, 2013.

978 Holben, B. N., Eck, T. F., Slutsker, I., Tanré, D., Buis, J. P., Setzer, A., Vermote, E., Reagan, J. A., Kaufman, Y. J.,
979 Nakajima, T., Lavenu, F., Jankowiak, I., and Smirnov, A.: AERONET—A Federated Instrument Network and Data
980 Archive for Aerosol Characterization, Remote Sens. Environ., 66(1), 1–16, doi:http://dx.doi.org/10.1016/S0034-
981 4257(98)00031-5, 1998.

982 Huang, J. P., Liu, J. J., Chen, B., and Nasiri, S. L.: Detection of anthropogenic dust using CALIPSO lidar
983 measurements, Atmos. Chem. Phys., 15(20), 11653–11665, doi:10.5194/acp-15-11653-2015, 2015.

984 IMPROVE: Reconstructing Light Extinction from Aerosol Measurements, Reconstr. Light Extinction from Aerosol
985 Meas. Interag. Monit. Prot. Vis. Environ. [online] Available from:
986 http://views.cira.colostate.edu/fed/DataWizard/Default.aspx (Accessed 20 May 2012), 2015.

987 IPCC: Climate Change 2013: The Physical Science Basis. Contribution of Working Group I to the Fifth Assessment
988 Report of the Intergovernmental Panel on Climate Change, 5th ed., edited by T. F. Stocker, D. Qin, G.-K. Plattner,
989 M. Tignor, S. K. Allen, J. Boschung, A. Nauels, Y. Xia, V. Bex, and P. M. Midgley, Cambridge University Press,
990 Cambridge, United Kingdom and New York, NY, USA., 2013.

991 Jasan, R. C., Plá, R. R., Invernizzi, R., and Dos Santos, M.: Characterization of atmospheric aerosol in Buenos
992 Aires, Argentina, J. Radioanal. Nucl. Chem., 281(1), 101–105, doi:10.1007/s10967-009-0071-1, 2009.

993 Jimenez, J. L., Canagaratna, M. R., Donahue, N. M., Prevot, A. S. H., Zhang, Q., Kroll, J. H., DeCarlo, P. F., Allan,
994 J. D., Coe, H., Ng, N. L., Aiken, A. C., Docherty, K. S., Ulbrich, I. M., Grieshop, A. P., Robinson, A. L., Duplissy,
995 J., Smith, J. D., Wilson, K. R., Lanz, V. A., Hueglin, C., Sun, Y. L., Tian, J., Laaksonen, A., Raatikainen, T.,
996 Rautiainen, J., Vaattovaara, P., Ehn, M., Kulmala, M., Tomlinson, J. M., Collins, D. R., Cubison, M. J., E., Dunlea,
997 J., Huffman, J. A., Onasch, T. B., Alfarra, M. R., Williams, P. I., Bower, K., Kondo, Y., Schneider, J., Drewnick, F.,
998 Borrmann, S., Weimer, S., Demerjian, K., Salcedo, D., Cottrell, L., Griffin, R., Takami, A., Miyoshi, T.,
999 Hatakeyama, S., Shimono, A., Sun, J. Y., Zhang, Y. M., Dzepina, K., Kimmel, J. R., Sueper, D., Jayne, J. T.,
1000 Herndon, S. C., Trimborn, A. M., Williams, L. R., Wood, E. C., Middlebrook, A. M., Kolb, C. E., Baltensperger, U.,
1001 and Worsnop, D. R.: Evolution of Organic Aerosols in the Atmosphere, Sci. , 326 (5959), 1525–1529,
1002 doi:10.1126/science.1180353, 2009.

1003 Kahn, R. A. and Gaitley, B. J.: An analysis of global aerosol type as retrieved by MISR, J. Geophys. Res. Atmos.,
1004 120(9), 4248–4281, doi:10.1002/2015JD023322, 2015.

1005 Kloog, I., Koutrakis, P., Coull, B. A., Lee, H. J., and Schwartz, J.: Assessing temporally and spatially resolved
1006 PM2.5 exposures for epidemiological studies using satellite aerosol optical depth measurements, Atmos. Environ.,
1007 45(35), 6267–6275, doi:10.1016/j.atmosenv.2011.08.066, 2011.

1008 Kloog, I., Ridgway, B., Koutrakis, P., Coull, B. A., and Schwartz, J. D.: Long- and Short-Term Exposure to PM(2.5)
1009 and Mortality: Using Novel Exposure Models, Epidemiology, 24(4), 555–561,
1010 doi:10.1097/EDE.0b013e318294beaa, 2013.

1011 Koepke, P., Hess, M., Schult, I., and Shettle, E. P.: Global Aerosol Dataset, Report N 243, Hamburg., 1997.

1012 Kreidenweis, S. M., Petters, M. D., and DeMott, P. J.: Single-parameter estimates of aerosol water content, Environ.

1013   Res. Lett., 3(3), 35002, doi:10.1088/1748-9326/3/3/035002, 2008.

1014   Laden, F., Schwartz, J., Speizer, F. E., and Dockery, D. W.: Reduction in Fine Particulate Air Pollution and
1015   Mortality, Am. J. Respir. Crit. Care Med., 173(6), 667–672, doi:10.1164/rccm.200503-443OC, 2006.

1016   Latham, J., Cumani, R., Rosati, I., and Bloise, M.: Global Land Cover SHARE (GLC-SHARE) database Beta-
1017   Release Version 1.0-2014, Rome., 2014.

1018   Lathem, T. L., Beyersdorf, A. J., Thornhill, K. L., Winstead, E. L., Cubison, M. J., Hecobian, A., Jimenez, J. L.,
1019   Weber, R. J., Anderson, B. E., and Nenes, A.: Analysis of CCN activity of Arctic aerosol and Canadian biomass
1020   burning during summer 2008, Atmos. Chem. Phys., 13(5), 2735–2756, doi:10.5194/acp-13-2735-2013, 2013.

1021   Lee, H. J., Coull, B. A., Bell, M. L., and Koutrakis, P.: Use of satellite-based aerosol optical depth and spatial
1022   clustering to predict ambient PM2.5 concentrations., Environ. Res., 118, 8–15, doi:10.1016/j.envres.2012.06.011,
1023   2012.

1024   Lelieveld, J., Evans, J. S., Fnais, M., Giannadaki, D., and Pozzer, A.: The contribution of outdoor air pollution
1025   sources to premature mortality on a global scale, Nature, 525(7569), 367–371, 2015.

1026   Lepeule, J., Laden, F., Dockery, D., and Schwartz, J.: Chronic Exposure to Fine Particles and Mortality: An
1027   Extended Follow-up of the Harvard Six Cities Study from 1974 to 2009, Environ. Health Perspect., 120(7), 965–
1028   970, doi:10.1289/ehp.1104660, 2012.

1029   Lestari, P., and Mauliadi, Y. D.: Source apportionment of particulate matter at urban mixed site in Indonesia using
1030   PMF, Atmos. Environ., 43(10), 1760–1770, doi:http://dx.doi.org/10.1016/j.atmosenv.2008.12.044, 2009.

1031   Lin, C., Li, Y., Yuan, Z., Lau, A. K. H., Li, C., and Fung, J. C. H.: Using satellite remote sensing data to estimate the
1032   high-resolution distribution of ground-level PM2.5, Remote Sens. Environ., 156, 117–128,
1033   doi:10.1016/j.rse.2014.09.015, 2015.

1034   Lippmann, M.: Toxicological and epidemiological studies of cardiovascular effects of ambient air fine particulate
1035   matter (PM2.5) and its chemical components: Coherence and public health implications, Crit. Rev. Toxicol., 44(4),
1036   299–347, doi:10.3109/10408444.2013.861796, 2014.

1037   Liu, Y., Monod, A., Tritscher, T., Praplan, A. P., DeCarlo, P. F., Temime-Roussel, B., Quivet, E., Marchand, N.,
1038   Dommen, J., and Baltensperger, U.: Aqueous phase processing of secondary organic aerosol from isoprene
1039   photooxidation, Atmos. Chem. Phys., 12(13), 5879–5895, doi:10.5194/acp-12-5879-2012, 2012.

1040   Malm, W. C., Sisler, J. F., Huffman, D., Eldred, R. A., and Cahill, T. A.: Spatial and seasonal trends in particle
1041   concentration and optical extinction in the United States, J. Geophys. Res., 99(D1), 1347–1370, 1994.

1042   Misra, A., Gaur, A., Bhattu, D., Ghosh, S., Dwivedi, A. K., Dalai, R., Paul, D., Gupta, T., Tare, V., Mishra, S. K.,
1043   Singh, S., and Tripathi, S. N.: An overview of the physico-chemical characteristics of dust at Kanpur in the central
1044   Indo-Gangetic basin, Atmos. Environ., 97, 386–396, doi:10.1016/j.atmosenv.2014.08.043, 2014.

1045   Munchak, L. A., Schichtel, B. A., Sullivan, A. P., Holden, A. S., Kreidenweis, S. M., Malm, W. C., and Collett, J.
1046   L.: Development of wildland fire particulate smoke marker to organic carbon emission ratios for the conterminous
1047   United States, Atmos. Environ., 45(2), 395–403, doi:10.1016/j.atmosenv.2010.10.006, 2011.

1048   Oanh, N. T. K., Upadhyay, N., Zhuang, Y.-H., Hao, Z.-P., Murthy, D. V. S., Lestari, P., Villarin, J. T., Chengchua,
1049   K., Co, H. X., Dung, N. T., and Lindgren, E. S.: Particulate air pollution in six Asian cities: Spatial and temporal
1050   distributions, and associated sources, Atmos. Environ., 40(18), 3367–3380,
1051   doi:http://dx.doi.org/10.1016/j.atmosenv.2006.01.050, 2006.

1052   Padró, L. T., Moore, R. H., Zhang, X., Rastogi, N., Weber, R. J., and Nenes, A.: Mixing state and compositional
1053   effects on CCN activity and droplet growth kinetics of size-resolved CCN in an urban environment, Atmos. Chem.
1054   Phys., 12(21), 10239–10255, doi:10.5194/acp-12-10239-2012, 2012.

1055   Patadia, F., Kahn, R. A., Limbacher, J. A., Burton, S. P., Ferrare, R. A., Hostetler, C. A., and Hair, J. W.: Aerosol
1056   airmass type mapping over the Urban Mexico City region from space-based multi-angle imaging, Atmos. Chem.
1057   Phys., 13(18), 9525–9541, doi:10.5194/acp-13-9525-2013, 2013.

1058   Petters, M. D. and Kreidenweis, S. M.: A single parameter representation of hygroscopic growth and cloud

1059   condensation nucleus activity, Atmos. Chem. Phys., 7(8), 1961–1971, doi:10.5194/acp-7-1961-2007, 2007.

1060   Petters, M. D. and Kreidenweis, S. M.: A single parameter representation of hygroscopic growth and cloud
1061   condensation nucleus activity – Part 2: Including solubility, Atmos. Chem. Phys., 8(20), 6273–6279,
1062   doi:10.5194/acp-8-6273-2008, 2008.

1063   Petters, M. D. and Kreidenweis, S. M.: A single parameter representation of hygroscopic growth and cloud
1064   condensation nucleus activity; Part 3: Including surfactant partitioning, Atmos. Chem. Phys., 13(2), 1081–1091,
1065   doi:10.5194/acp-13-1081-2013, 2013.

1066   Petzold, A., Ogren, J. A., Fiebig, M., Laj, P., Li, S.-M., Baltensperger, U., Holzer-Popp, T., Kinne, S., Pappalardo,
1067   G., Sugimoto, N., Wehrli, C., Wiedensohler, A., and Zhang, X.-Y.: Recommendations for reporting "black carbon"
1068   measurements, Atmos. Chem. Phys., 13(16), 8365–8379, doi:10.5194/acp-13-8365-2013, 2013.

1069   Philip, S., Martin, R. V, van Donkelaar, A., Lo, J. W.-H., Wang, Y., Chen, D., Zhang, L., Kasibhatla, P. S., Wang,
1070   S., Zhang, Q., Lu, Z., Streets, D. G., Bittman, S., and Macdonald, D. J.: Global Chemical Composition of Ambient
1071   Fine Particulate Matter for Exposure Assessment, Environ. Sci. Technol., 48(22), 13060–13068,
1072   doi:10.1021/es502965b, 2014a.

1073   Philip, S., Martin, R. V., Pierce, J. R., Jimenez, J. L., Zhang, Q., Canagaratna, M. R., Spracklen, D. V., Nowlan, C.
1074   R., Lamsal, L. N., Cooper, M. J., and Krotkov, N. A.: Spatially and seasonally resolved estimate of the ratio of
1075   organic mass to organic carbon, Atmos. Environ., 87, 34–40, doi:10.1016/j.atmosenv.2013.11.065, 2014b.

1076   Pitchford, M., Malm, W., Schichtel, B., Kumar, N., Lowenthal, D., and Hand, J.: Revised Algorithm for Estimating
1077   Light Extinction from IMPROVE Particle Speciation Data, J. Air Waste Manage. Assoc., 57(11), 1326–1336,
1078   doi:10.3155/1047-3289.57.11.1326, 2007.

1079   Prenni, A. J., Petters, M. D., Kreidenweis, S. M., DeMott, P. J., and Ziemann, P. J.: Cloud droplet activation of
1080   secondary organic aerosol, J. Geophys. Res., 112(D10), D10223, doi:10.1029/2006JD007963, 2007.

1081   Putaud, J.-P., Raes, F., Van Dingenen, R., Brüggemann, E., Facchini, M.-C., Decesari, S., Fuzzi, S., Gehrig, R.,
1082   Hüglin, C., Laj, P., Lorbeer, G., Maenhaut, W., Mihalopoulos, N., Müller, K., Querol, X., Rodriguez, S., Schneider,
1083   J., Spindler, G., Brink, H. ten, Tørseth, K., and Wiedensohler, A.: A European aerosol phenomenology—2: chemical
1084   characteristics of particulate matter at kerbside, urban, rural and background sites in Europe, Atmos. Environ.,
1085   38(16), 2579–2595, doi:http://dx.doi.org/10.1016/j.atmosenv.2004.01.041, 2004.

1086   Putaud, J.-P., Van Dingenen, R., Alastuey, A., Bauer, H., Birmili, W., Cyrys, J., Flentje, H., Fuzzi, S., Gehrig, R.,
1087   Hansson, H. C., Harrison, R. M., Herrmann, H., Hitzenberger, R., Hüglin, C., Jones, A. M., Kasper-Giebl, A., Kiss,
1088   G., Kousa, A., Kuhlbusch, T. A. J., Löschau, G., Maenhaut, W., Molnar, A., Moreno, T., Pekkanen, J., Perrino, C.,
1089   Pitz, M., Puxbaum, H., Querol, X., Rodriguez, S., Salma, I., Schwarz, J., Smolik, J., Schneider, J., Spindler, G., ten
1090   Brink, H., Tursic, J., Viana, M., Wiedensohler, A., and Raes, F.: A European aerosol phenomenology – 3: Physical
1091   and chemical characteristics of particulate matter from 60 rural, urban, and kerbside sites across Europe, Atmos.
1092   Environ., 44(10), 1308–1320, doi:10.1016/j.atmosenv.2009.12.011, 2010.

1093   Quincey, P., Butterfield, D., Green, D., Coyle, M., and Cape, J. N.: An evaluation of measurement methods for
1094   organic, elemental and black carbon in ambient air monitoring sites, Atmos. Environ., 43(32), 5085–5091,
1095   doi:http://dx.doi.org/10.1016/j.atmosenv.2009.06.041, 2009.

1096   Ram, K., Sarin, M. M., and Tripathi, S. N.: Temporal Trends in Atmospheric PM2.5, PM10, Elemental Carbon,
1097   Organic Carbon, Water-Soluble Organic Carbon, and Optical Properties: Impact of Biomass Burning Emissions in
1098   The Indo-Gangetic Plain, Environ. Sci. Technol., 46(2), 686–695, doi:10.1021/es202857w, 2012.

1099   Remoundaki, E., Kassomenos, P., Mantas, E., Mihalopoulos, N., and Tsezos, M.: Composition and Mass Closure of
1100   PM2.5 in Urban Environment (Athens, Greece), Aerosol Air Qual. Res., 13(1), 72–82, 2013.

1101   Rickards, A. M. J., Miles, R. E. H., Davies, J. F., Marshall, F. H., and Reid, J. P.: Measurements of the Sensitivity of
1102   Aerosol Hygroscopicity and the κ Parameter to the O/C Ratio, J. Phys. Chem. A, 117(51), 14120–14131,
1103   doi:10.1021/jp407991n, 2013.

1104   Robinson, C. B., Schill, G. P., Zarzana, K. J., and Tolbert, M. A.: Impact of Organic Coating on Optical Growth of
1105   Ammonium Sulfate Particles, Environ. Sci. Technol., 47(23), 13339–13346, doi:10.1021/es4023128, 2013.

1106   Santoso, M., Dwiana Lestiani, D., and Hopke, P. K.: Atmospheric black carbon in PM2.5 in Indonesian cities, J. Air
1107   Waste Manage. Assoc., 63(9), 1022–1025, doi:10.1080/10962247.2013.804465, 2013.

1108   Snider, G., Weagle, C. L., Martin, R. V., van Donkelaar, A., Conrad, K., Cunningham, D., Gordon, C., Zwicker, M.,
1109   Akoshile, C., Artaxo, P., Anh, N. X., Brook, J., Dong, J., Garland, R. M., Greenwald, R., Griffith, D., He, K.,
1110   Holben, B. N., Kahn, R., Koren, I., Lagrosas, N., Lestari, P., Ma, Z., Vanderlei Martins, J., Quel, E. J., Rudich, Y.,
1111   Salam, A., Tripathi, S. N., Yu, C., Zhang, Q., Zhang, Y., Brauer, M., Cohen, A., Gibson, M. D., and Liu, Y.:
1112   SPARTAN: a global network to evaluate and enhance satellite-based estimates of ground-level particulate matter for
1113   global health applications, Atmos. Meas. Tech., 8(1), 505–521, doi:10.5194/amt-8-505-2015, 2015.

1114   Sorooshian, A., Hersey, S., Brechtel, F. J., Corless, A., Flagan, R. C., and Seinfeld, J. H.: Rapid, Size-Resolved
1115   Aerosol Hygroscopic Growth Measurements: Differential Aerosol Sizing and Hygroscopicity Spectrometer Probe
1116   (DASH-SP), Aerosol Sci. Technol., 42(6), 445–464, doi:10.1080/02786820802178506, 2008.

1117   Sun, Y.-L., Zhang, Q., Schwab, J. J., Demerjian, K. L., Chen, W.-N., Bae, M.-S., Hung, H.-M., Hogrefe, O., Frank,
1118   B., Rattigan, O. V., and Lin, Y.-C.: Characterization of the sources and processes of organic and inorganic aerosols
1119   in New York city with a high-resolution time-of-flight aerosol mass apectrometer, Atmos. Chem. Phys., 11(4),
1120   1581–1602, doi:10.5194/acp-11-1581-2011, 2011.

1121   Svenningsson, B., Rissler, J., Swietlicki, E., Mircea, M., Bilde, M., Facchini, M. C., Decesari, S., Fuzzi, S., Zhou, J.,
1122   Mønster, J., and Rosenørn, T.: Hygroscopic growth and critical supersaturations for mixed aerosol particles of
1123   inorganic and organic compounds of atmospheric relevance, Atmos. Chem. Phys., 6(7), 1937–1952,
1124   doi:10.5194/acp-6-1937-2006, 2006.

1125   Swietlicki, E., Hansson, H.-C., Hämeri, K., Svenningsson, B., Massling, A., McFiggans, G., McMurry, P. H., Petäjä,
1126   T., Tunved, P., Gysel, M., Topping, D., Weingartner, E., Baltensperger, U., Rissler, J., Wiedensohler, A., and
1127   Kulmala, M.: Hygroscopic properties of submicrometer atmospheric aerosol particles measured with H-TDMA
1128   instruments in various environments—a review, Tellus B, 60(3), 432–469, 2008.

1129   Taha, G., Box, G. P., Cohen, D. D., and Stelcer, E.: Black Carbon Measurement using Laser Integrating Plate
1130   Method, Aerosol Sci. Technol., 41(3), 266–276, doi:10.1080/02786820601156224, 2007.

1131   USEPA: Chemical Speciation Network Database, [online] Available from:
1132   http://views.cira.colostate.edu/fed/DataWizard/Default.aspx (Accessed 1 December 2015), 2015.

1133   Varutbangkul, V., Brechtel, F. J., Bahreini, R., Ng, N. L., Keywood, M. D., Kroll, J. H., Flagan, R. C., Seinfeld, J.
1134   H., Lee, A., and Goldstein, A. H.: Hygroscopicity of secondary organic aerosols formed by oxidation of
1135   cycloalkenes, monoterpenes, sesquiterpenes, and related compounds, Atmos. Chem. Phys., 6(9), 2367–2388,
1136   doi:10.5194/acp-6-2367-2006, 2006.

1137   Villalobos, A. M., Amonov, M. O., Shafer, M. M., Devi, J. J., Gupta, T., Tripathi, S. N., Rana, K. S., Mckenzie, M.,
1138   Bergin, M. H., and Schauer, J. J.: Source apportionment of carbonaceous fine particulate matter (PM2.5) in two
1139   contrasting cities across the Indo–Gangetic Plain, Atmos. Pollut. Res., 6(3), 398, 2015.

1140   Vu Van, H., Le Xuan, Q., Pham Ngoc, H., and Luc, H.: Health Risk Assessment of Mobility-Related Air Pollution
1141   in Ha Noi, Vietnam, J. Environ. Prot. (Irvine,. Calif)., 4(10), 1165–1172, 2013.

1142   Wagner, F., Bortoli, D., Pereira, S., João Costa, M., Silva, A. M., Weinzierl, B., Esselborn, M., Petzold, A., Rasp,
1143   K., Heinold, B., and Tegen, I.: Properties of dust aerosol particles transported to Portugal from the Sahara desert,
1144   Tellus B, 61(1), 297–306, 2009.

1145   Wang, J. L.: Mapping the Global Dust Storm Records: Review of Dust Data Sources in Supporting
1146   Modeling/Climate Study, Curr. Pollut. Reports, 1(2), 82–94, doi:10.1007/s40726-015-0008-y, 2015.

1147   Wang, Z., Chen, L., Tao, J., Zhang, Y., and Su, L.: Satellite-based estimation of regional particulate matter (PM) in
1148   Beijing using vertical-and-RH correcting method, Remote Sens. Environ., 114(1), 50–63,
1149   doi:http://dx.doi.org/10.1016/j.rse.2009.08.009, 2010.

1150   Wexler, A. S. and Clegg, S. L.: Atmospheric aerosol models for systems including the ions H+, NH4+, Na+, SO42−,
1151   NO3−, Cl−, Br−, and H2O, J. Geophys. Res. Atmos., 107(D14), ACH14–1–14, doi:10.1029/2001JD000451, 2002.

1152   WHO: Human exposure to air pollution, in Update of the World Air Quality Guidelines World Health Organization,

1153   pp. 61–86, World Health Organization, Geneva, Switzerland., 2005.

1154   WHO: WHO | Air quality guidelines - global update 2005, World Health Organization, Geneva, Switzerland., 2006.

1155   Wise, M. E., Surratt, J. D., Curtis, D. B., Shilling, J. E., and Tolbert, M. A.: Hygroscopic growth of ammonium
1156   sulfate/dicarboxylic acids, J. Geophys. Res. Atmos., 108(D20), 4638, doi:10.1029/2003JD003775, 2003.

1157   Yang, F., Tan, J., Zhao, Q., Du, Z., He, K., Ma, Y., Duan, F., and Chen, G.: Characteristics of PM$_{2.5}$ speciation in
1158   representative megacities and across China, Atmos. Chem. Phys., 11(11), 5207–5219, doi:10.5194/acp-11-5207-
1159   2011, 2011.

1160   Zhang, R., Jing, J., Tao, J., Hsu, S.-C., Wang, G., Cao, J., Lee, C. S. L., Zhu, L., Chen, Z., Zhao, Y., and Shen, Z.:
1161   Chemical characterization and source apportionment of PM$_{2.5}$ in Beijing: seasonal perspective, Atmos. Chem. Phys.,
1162   13(14), 7053–7074, doi:10.5194/acp-13-7053-2013, 2013.

1163   Zhang, W.-J., Sun, Y.-L., Zhuang, G.-S., and Xu, D.-Q.: Characteristics and seasonal variations of PM2.5, PM10,
1164   and TSP aerosol in Beijing, Biomed. Environ. Sci., 19(6), 461–468, 2006.

1165

1166

Figures and Tables

Table 1: Summary of speciation definitions

Species (at 0% RH)	Measurement Method	Species Mass (µg). For concentrations, divide masses by sampling volume v	Reference
SS	IC (anion and cation)	$2.54[Na^+]_{SS}$, where $[Na^+]_{SS} = [Na^+]_{tot} - 0.1[Al]$	(Remoundaki et al., 2013) (Malm et al., 1994)
ANO₃		$1.29[NO_3^-]$	(Malm et al., 1994)
ASO₄		$[SO_4^{2-}]_{non-ss} + [NH_4^+] - 0.29[NO_3^-]$, where $[SO_4^{2-}]_{non-ss} = [SO_4^{2-}]_{total} - 0.12[Na^+]$	(Dabek-Zlotorzynska et al., 2011; Henning et al., 2003)
Na₂SO₄		$0.18[Na^+]_{SS}$	
CM	ICP-MS & IC	$10 \times ([Al] + [Mg] + [Fe])$	(Wang, 2015)
EBC	SSR	$20.7 \times \ln(R_o/R)$	(Taha et al., 2007)
TEO	ICP-MS	$1.47[V] + 1.27[Ni] + 1.25[Cu] + 1.24[Zn] + 1.32[As] + 1.2[Se] + 1.07[Ag] + 1.14[Cd] + 1.2[Sb] + 1.12[Ba] + 1.23[Ce] + 1.08[Pb]$	(Malm et al., 1994)
PBW$_{inorg}$	$\kappa_{m,X}$	$\sum_X [f_{m,X}(RH) - 1][X]$	(Kreidenweis et al., 2008)
PBW$_{RM}$		$RM(1 - 1/f_{m,RM})$	Table 2
RM(35%)	Mass Balance	$[PM_{2.5}] - \{[EBC] + [CM] + [TEO] + [ANO_3] + [SS] + [ASO_4] + [Na_2SO_4] + [PBW]_{inorg}\}$	This Study
RM(0%)	Mass Balance $\kappa_{m,OM} = 0.07$	$RM(35\%) - PBW_{RM}$	Organic growth factors: (Jimenez et al., 2009; Sun et al., 2011)

Species: EBC = Equivalent black carbon, TEO = Trace metal oxides, CM = Crustal Material, ANO₃ = Ammonium nitrate, ASO₄ = Ammoniated sulfate, PBW = particle-bound water, RM = residual matter (assumed representative of organic matter), [X] = concentration of any hygroscopic species. **Measurement Instruments:** IC = Ion Chromatography, ICP-MS Inductively coupled plasma mass spectrometry, SSR = Smoke Stain Reflectometer, $\kappa_{m,X}$ = single-parameter hygroscopicity by mass (Kreidenweis et al., 2008). RH = Relative Humidity,

Table 2: κ-Kohler constants for volume (κ$_v$), mass (κ$_m$), and related quantities

Compound [X]	$\kappa_{v,X}$	Approximate Density (ρ_X/ρ_{water})	$\kappa_{m,X}$	PBW(%mass) at RH = 35%	PBW(%mass) at RH = 80%
Crustal	0	2.5[a]	0	0	0
EBC	0	1.8[b]	0	0	0
TEO	0	2.5	0	0	0
RM	0.1[c]	1.4	0.07	2	12
ANO₃	0.41	1.72	0.24	17	61
ASO₄	0.51	1.76	0.29	15	56
Na₂SO₄	0.68[d]	2.68[d]	0.25	12	50
SS	1.5[e]	2.16	0.69	22	68

PBW = Particle-bound water. EBC = Equivalent black carbon, TEO = Trace Element Oxides, RM = Residue Matter (associated with organics), ANO₃ = ammonium nitrate, ASO₄ = Ammoniated sulfate. [a] Wagner et al. (2009), [b] Bond and Bergstrom (2006), [c] Assuming an urban O:C ratio of 0.5 then $\kappa_{v,OM} = 0.1$ Jimenez et al. (2009), [d] Petters and Kreidenweis (2007). [e] Fitted using non-deliquesced, subsaturated AIM Model III values, plus 0% RH endpoint by Kreidenweis et al. (2008).

Table 3: PM$_{2.5}$ composition and water content (µg m^{-3}) at each SPARTAN location.

City	Host Institute	Lat/Lon (°)	Elev./Inst. Elev. (m)	Filters (n)	ASO$_4$	ANO$_3$	CM	SS	EBC	TEO	RM	PBW 35%RH	ρ 0%RH (g/cm^3)	NO$_3$ vs. NH$_4^+$ (r^2)	PM$_{2.5}$	PM$_{2.5}$/PM$_{10}$	κ$_{v,tot}$	PM$_{2.5}$ K/Al	Zn/Al	Filter Sampling Period
Beijing	Tsinghua University	40.010, 116.333	60// 7.5	114	12.0 (7.9)	5.5 (6.4)	15.9 (8.8)	1.5 (2.1)	5.7 (3.4)	0.62 (0.51)	23.8 (18)	4.7 (2.8)	1.69	0.32	69.5 (2.5)	0.49	0.19	2.9	0.51	2013/06 –2016/02
Bandung	ITB Bandung	-6.888, 107.610	826// 20	77	6.0 (2.3)	0.7 (1.3)	2.5 (1.5)	0.3 (0.2)	3.7 (2.0)	0.14 (0.11)	16.0 (5.9)	1.9 (0.6)	1.55	0.06	31.4 (1.0)	0.58	0.17	6.8	0.52	2014/01 –2015/11
Manila	Manila Observatory	14.635, 121.080	60// 10	63	2.7 (1.5)	0.3 (0.2)	1.9 (1.0)	0.5 (0.4)	4.3 (3.3)	0.13 (0.13)	7.3 (3.5)	1.1 (0.5)	1.61	0.03	18.2 (0.8)	0.39	0.16	6.3	1.03	2014/02 – 2016/01
Dhaka	Dhaka University	23.728, 90.398	20// 20	41	7.5 (4.3)	2.1 (1.8)	5.9 (4.0)	1.4 (1.7)	8.4 (5.1)	1.50 (1.46)	21.4 (16)	3.5 (2.2)	1.63	0.43	51.9 (3.7)	0.40	0.17	5.3	3.39	2014/05 –2015/11
Ilorin	Ilorin University	8.484, 4.675	330// 10	40	1.9 (0.8)	0.3 (0.1)	3.0 (2.2)	0.3 (0.4)	1.6 (0.8)	0.09 (0.07)	7.6 (3.8)	0.9 (0.4)	1.62	0.05	15.7 (0.8)	0.44	0.15	2.9	0.49	2014/03 – 2015/10
Kanpur	IIT Kanpur	26.519, 80.233	130// 10	33	17.6 (12)	6.8 (5.3)	4.4 (2.3)	0.6 (0.3)	8.3 (4.7)	0.47 (0.36)	54.6 (33)	6.3 (3.6)	1.52	0.58	99.3 (9.1)	0.56	0.18	16.2	1.01	2013/12 – 2014/11
Buenos Aires	CITEDEF	-34.560, -58.506	25// 7	31	1.1 (0.5)	0.8 (0.4)	2.2 (1.6)	0.6 (0.3)	1.7 (1.2)	0.12 (0.12)	3.1 (1.8)	0.9 (0.3)	1.70	0.28	10.1 (0.6)	0.39	0.19	2.7	0.44	2014/10 – 2016/02
Rehovot	Weizmann Institute	31.907, 34.810	20// 10	30	4.7 (1.9)	0.9 (0.5)	3.3 (1.6)	0.7 (0.6)	2.2 (2.0)	0.12 (0.13)	2.6 (2.8)	1.6 (0.6)	1.79	0.01	16.1 (1.0)	0.40	0.28	2.7	0.40	2015/02 –2016/02
Mammoth Cave NP	Mammoth Cave	37.132, -86.148	235// 7	19	4.1 (2.4)	0.2 (0.1)	1.4 (1.4)	0.1 (0.1)	0.7 (0.4)	0.02 (0.03)	6.1 (4.3)	1.0 (0.5)	1.59	0.00	13.6 (1.8)	0.56	0.22	1.1	0.13	2014/04- 2014/08
Atlanta	Emory University	33.688, -84.290	250// 2	13	2.0 (0.9)	0.3 (0.1)	1.0 (0.4)	0.1 (0.1)	1.1 (1.0)	0.04 (0.02)	4.1 (1.8)	0.6 (0.2)	1.61	0.00	9.1 (0.7)	0.69	0.17	1.9	0.26	2014/01 –2014/05
Singapore	NUS	1.298, 103.780	10// 20	12	16.1 (6.5)	1.2 (0.9)	0.8 (0.3)	0.9 (0.4)	3.1 (2.7)	0.20 (0.16)	39.8 (29)	5.0 (2.4)	1.48	0.66	66.8 (11)	NA	0.21	13.2	1.53	2015/08 – 2015/12
Hanoi	Vietnam Acad. Sci.	21.048, 105.800	10// 20	10	6.0 (2.1)	1.6 (0.4)	5.6 (5.4)	0.9 (0.2)	3.7 (2.1)	0.69 (0.43)	18.2 (7.8)	2.6 (0.7)	1.59	0.22	39.4 (3.9)	0.38	0.18	8.9	3.74	2015/05 – 2015/08
Pretoria	CSIR	-25.756, 28.280	1310// 10	5	1.2 (1.6)	0.7 (0.3)	1.3 (1.8)	0.2 (0.1)	1.4 (0.9)	0.04 (0.04)	1.0 (0.7)	0.5 (0.4)	2.09	0.48	6.4 (2.3)	0.32	0.24	6.0	0.86	2015/09- 2015/11
SPARTAN mean (% mass)	**All sites**			497	20 (11)%	4.7 (3.0)%	13.4 (9.9)%	2.3 (1.6)%	11.9 (8.4)%	1.0 (1.1)%	40 (24)%	7.2 (3.3)%	1.65	0.24	32.4 (2.9)	0.50	0.20	4.6	0.73	2013 – 2016

[a]Values in parentheses are 1σ standard deviations. RH = Relative Humidity, ANO$_3$ = ammonium nitrate, ASO$_4$ = Ammoniated sulfate, CM = Crustal material, EBC = Equivalent black carbon, TEO = Trace Element Oxides, RM = Residue Matter, PBW = Particle-bound water. Mean Na$_2$SO$_4$ was not significant (< 0.1 µg m^{-3}) at any SPARTAN site. [b]Geometric mean of ratio
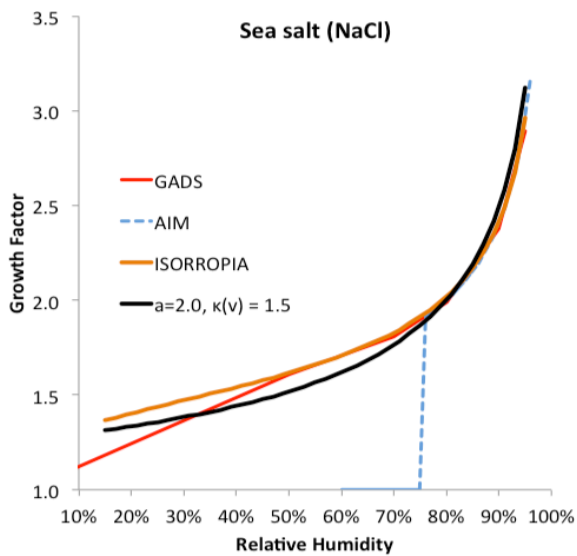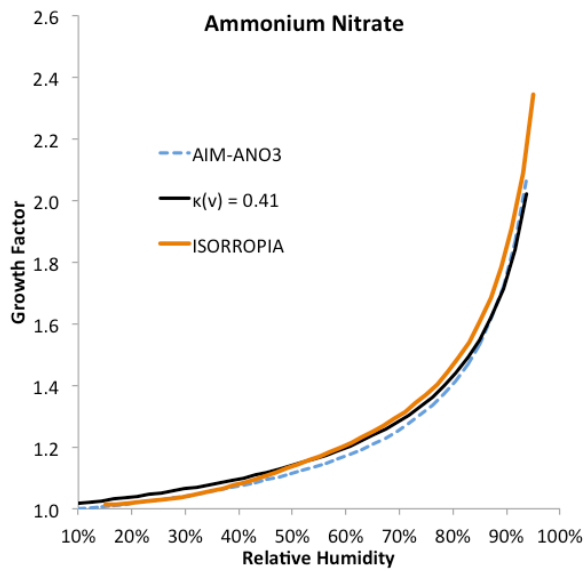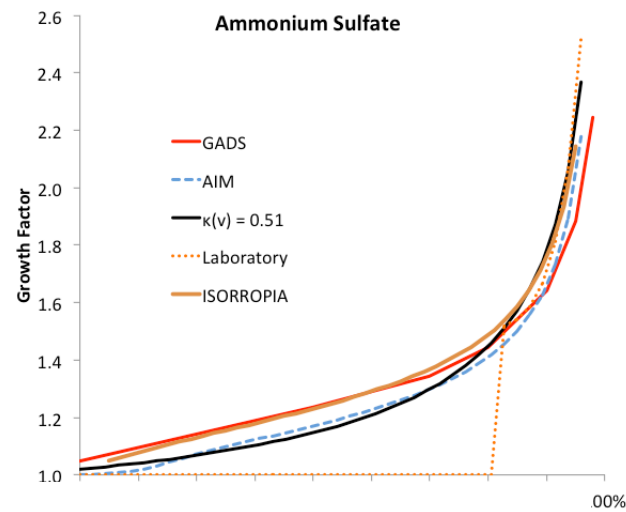
Figure 1: Hygroscopic growth factors for ASO₄ (top), ANO₃ (centre), and sea salt (bottom). GADS = Global Aerosol Dataset estimated from empirical data (Koepke et al., 1997)**. ISORROPIA = Aerosol thermodynamic model at T=298K (reverse mode) and assuming linear water/solvent volume additivity** (Fountoukis and Nenes, 2007)**. AIM = Aerosol Inorganic Model calculated metastable growth for ASO₄ and ANO₃ at T=298K** (Wexler and Clegg, 2002)**, Laboratory ASO₄ fit is $GF = 1.49 + 2.81 \cdot RH^{24.6}$ (with deliquescence at 80%) for bulk pure ASO₄** (Wise et al., 2003)**. All components are fit using Eq 6.**
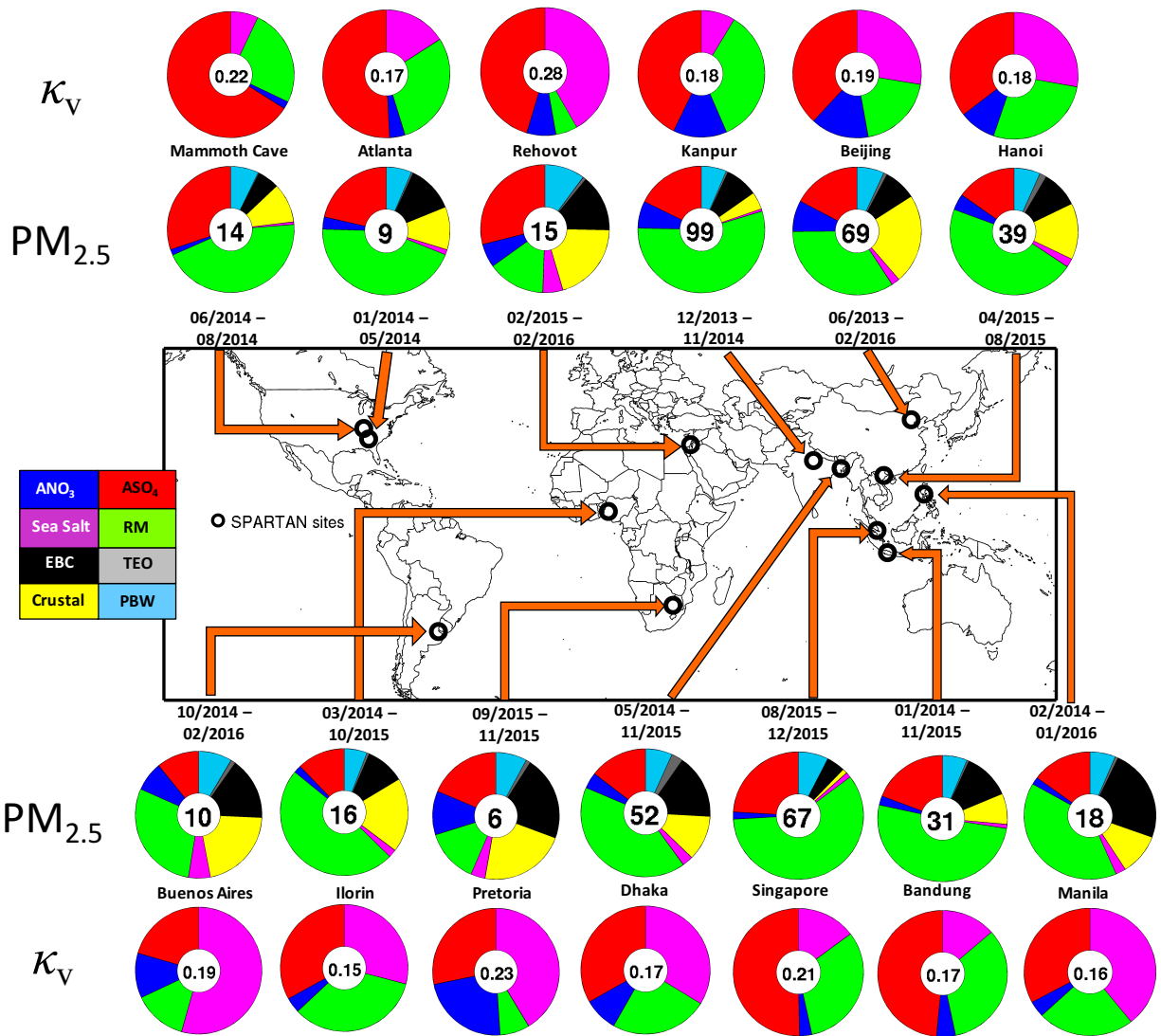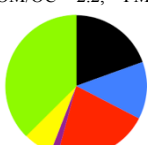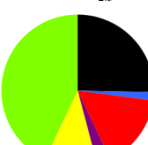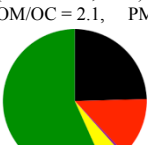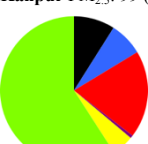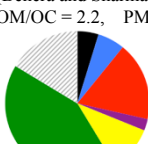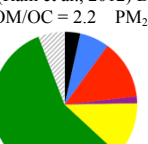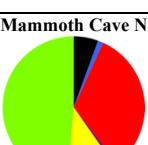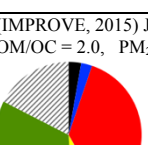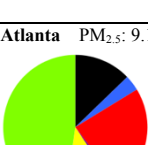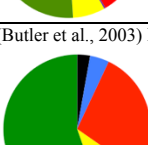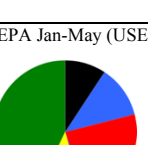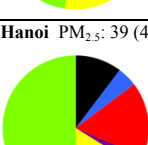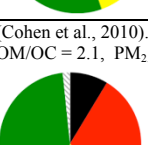
Figure 2: PM$_{2.5}$ mass (inner circle, μg m^{-3}) and composition mass fraction (filled colors) is shown in interior pie charts. Exterior pie charts contain site-mean κ_v surrounded by the relative contribution of PBW water at 35% RH.

Figure 3: Comparison of SPARTAN water-free aerosol composition with 11 collocated speciation studies. The numbers in parentheses show 1-σ deviations of averaged masses. The number of filters sampled is *n*. Dark green = organic, Light green = residual, black = equivalent black carbon, red = Ammoniated sulfate, blue = ammonium nitrate, purple = sea salt, yellow = crustal, and grey stripes = unknown. OM/OC ratios are from Philip et al. (2014b) and Canagaratna et al. (2015). Relative mass percentages are based on water-free aerosol components. SPARTAN percentages are renormalized to 100% after omission of species not found in comparison studies.

$PM_{2.5}$ mass = µg m^{-3} (1σ/√n), components = % (1σ)		
This study (total mass = µg m^{-3})	**Prior Study (µg m^{-3})**	**Prior Study (µg m^{-3})**
Beijing $PM_{2.5}$: 69 (3), *n* = 114 8.5 (10)% ANO_3, 19 (12)% ASO_4, 2.3 (3.3)% SS, 25 (14)% CM, 8.8 (5.3)% EBC, 37 (27)% RM	(Yang et al., 2011) 2005-2006, OM/OC = 1.7, $PM_{2.5}$: 119(40) 11 (7)% ANO_3, 17 (10)% ASO_4, 1.3 (0.6)% SS, 19 (3)% CM, 7 (5)% EC, 33 (16)% OM, 10 (10)% Unk	(Oanh et al., 2006) 2001-2004, OM/OC = 1.7 $PM_{2.5}$: 136 (45) 12 (1.5)% ANO_3, 20 (1.8)% ASO_4, 1.2 (1.2)% SS, 5 (3)% CM, 9 (7)% EBC, 29 (22)% OM, 24 (24)% Unk
Bandung $PM_{2.5}$: 31 (1), *n* = 77 2.4 (1.4)% ANO_3, 21 (8)% ASO_4, 1.0 (0.3)% SS, 8.6 (4.1)% CM, 13 (4)% EBC, 55 (19)% RM	(Oanh et al., 2006) 2001-2004. OM/OC = 2.2, $PM_{2.5}$: 45.5(10.6), 13(4)% ANO_3, 21(3)% ASO_4, 1.6(0.2)% SS, 6.6(0.5)% CM, 19 (4)% EBC, 36(11)% RM	(Lestari and Mauliadi, 2009) 2001- 2007, OM/OC = 2.2 $PM_{2.5}$: 43.5(10.5) 4(6)% ANO_3, 4(4)% ASO_4, 3(2)% SS, 23(21)% CM, 24(14)% EBC, 42(35)% RM
Manila $PM_{2.5}$: 18 (1), *n* = 63 1.8 (1.2)% ANO_3, 16 (9)% ASO_4, 2.9 (2.4)% SS, 11 (6)% CM, 25 (19)% EBC, 43 (21)% RM	(Cohen et al., 2009) 2001-2007, OM/OC = 2.1, $PM_{2.5}$: 46 (19), ANO_3 N/A 14 (9)% ASO_4, 0.6 (1.5)% SS, 5 (1.7)% CM, 25 (11)% EBC, 57(22)% OM,	
Kanpur $PM_{2.5}$: 99 (9), *n* = 33 7.4 (5.7)% ANO_3, 19 (13)% ASO_4, 0.7 (0.3)% SS, 4.8 (2.9)% CM, 9 (5.0)% EBC, 59 (35)% RM	(Behera and Sharma, 2010) Oct. 2007 – Jan. 2008, OM/OC = 2.2, $PM_{2.5}$: 172 (73), 6.1 (1.3)% ANO_3, 18 (4)% ASO_4, 2.6 (0.6)% SS, 10 (3)% CM, 4.8 (1.1)% EC, 42 (9)% OM, 16 (10)% Unk	(Ram et al., 2012) Dec 2008 – Feb 2009, OM/OC = 2.2 $PM_{2.5}$: 158 (47) 6.6(4)% ANO_3, 13 (5)% ASO_4, 1.5 (0.9)% SS, 12 (6)% CM* 3 (1.1)% EC, 57 (23)% OM, 6 (24)% Unk *Assuming CM = [Ca]/0.034 (Wang, 2015)
Mammoth Cave NP $PM_{2.5}$: 13.6 (2), *n* = 19 1.2 (1.0)% ANO_3, 33 (19)% ASO_4, 0.8 (0.8)% SS, 11 (11)% CM, 5.6 (3.2)% EBC, 49 (34)% RM	(IMPROVE, 2015) June-Aug. 2014, OM/OC = 2.0, $PM_{2.5}$: 10.0 (5.8), 2.4 (2.5)% ANO_3, 36 (17)% ASO_4, 0.3 (1.6)% SS, 7 (8)% CM, 3 (3)% EC, 34 (30)% OM, 17% Unk+H_2O	
Atlanta $PM_{2.5}$: 9.1 (1), *n* = 13 3.5 (1.2)% ANO_3, 23 (11)% ASO_4, 1.2 (1.2)% SS, 12 (4.7)% CM, 11 (2.6)% EBC, 48 (25)% RM	(Butler et al., 2003) Mar. 1999 –2000 Feb, OM/OC = 2.0, $PM_{2.5}$: 24.2 4 (0.2)% ANO_3, 28 (1.0)% ASO_4, 10 (0.8)% CM, 3 (0.2)% EC, 55 (5)% OM,	EPA Jan-May (USEPA, 2015), OM/OC = 2.0 $PM_{2.5}$: 8.5 12 (5)% ANO_3, 23 (15)% ASO_4, 1.4 (0.6)% SS 12 (5)% CM, 9.3 (5)% EC, 43 (36)% OM,
Hanoi $PM_{2.5}$: 39 (4), *n* = 10 4.4 (1.1)% ANO_3, 17 (6)% ASO_4, 2.5 (0.6)% SS, 16 (15)% CM, 10 (5.8)% EBC, 51 (22)% RM	(Cohen et al., 2010). 2001 –2008 OM/OC = 2.1, $PM_{2.5}$: 54 (33) ANO_3 N/A 29 (20)% ASO_4, 0.6 (1.4)%SS 13 (7)% CM, 8 (3)% EBC, 40 (19)% OM, 2 (2)% Unk + ANO_3	
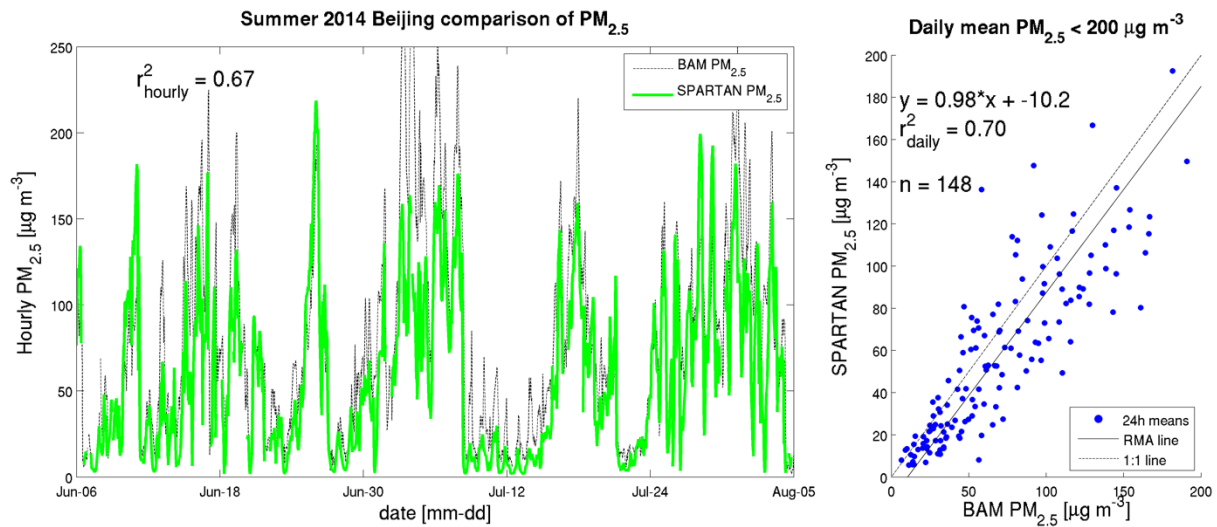
Figure 4: Left Hourly PM$_{2.5}$ estimated from SPARTAN overlaid with a MetOne BAM-1020 (June-August 2014) at the Beijing US Embassy (15 km away). Right: 24-hour SPARTAN PM$_{2.5}$ compared with BAM for the year 2014. Reduced major axis (RMA) slope and Pearson correlations for PM$_{2.5}$ are given in inset.

Appendix:

Appendix A1:

Table A1: Hygroscopicity parameter κ_v for various studies on organic material

κ_v (OM)	Comments	Reference
0.045	Fitted to an aged organic mixture, subsaturated	(Varutbangkul et al., 2006)
0	IMPROVE network, subsaturated	(Hand and Malm, 2006)
0.10 ± 0.04	RH > 99%, fitted to SOA precursors	(Prenni et al., 2007)
$-0.067 + 0.33$(O:C)	Fitted, RH > 99%	(Jimenez et al., 2009)
0.29(O:C)	RH > 99%, 0.3 < O:C < 0.6	(Chang et al., 2010)
0.05	Best estimate from aged mixtures, subsaturated	(Dusek et al., 2011)
0.01 – 0.2	Field studies & smog chamber, subsaturated	(Duplissy et al., 2011)
0.16	RH > 99%	(Asa-Awuku et al., 2011)
0.05 – 0.13	Lab experiments, aged with H_2O_2 and light; subsaturated	(Liu et al., 2012)
0.1	RH > 99%, D_{dry} < 100 nm	(Padró et al., 2012)
$0.12\varepsilon_{WSOM}$[#]	RH > 99%	(Lathem et al., 2013)
$-0.005 + 0.19$(O:C)	Fitted, RH > 99% 100 nm particle	(Rickards et al., 2013)
0.03, 0.1	HDTMA-measure, subsaturated	(Bezantakos et al., 2013)
0.1	Subsaturated	Selected for this study

[#]ε_{WSOM} = fraction of water-soluble organic material.

Appendix A2:

Dry aerosol scatter ($b_{sp,\text{dry}}$) is related to relative humidity (RH) by

$$b_{sp,\text{dry}} = \frac{b_{sp}(\text{RH})}{f_v(\text{RH})} \qquad\qquad \text{Eq. A1}$$

Changes in scatter are also proportional to mass (Chow et al., 2006; Wang et al., 2010)

$$b_{sp,\text{dry}} = \alpha \text{PM}_{2.5,\text{dry}} \qquad\qquad \text{Eq. A2}$$

where α (m^2 g^{-1}) is the mass scattering efficiency and a function of aerosol size distribution, effective radius, and dry composition. In this study we treat composition, density, and size distribution as constant over each of our 9-day intermittent sampling periods so that $\alpha \approx \langle\alpha\rangle_{9d}$. Under this assumption the predicted mass changes in low humidity (35% RH) are proportional to water-free aerosol scatter:

$$\text{PM}_{2.5,\text{dry}} = \langle\text{PM}_{2.5,\text{dry}}\rangle \frac{b_{sp,\text{dry}}}{\langle b_{sp,\text{dry}}\rangle} \qquad\qquad \text{Eq. A3}$$

where $<>$ indicates 9-day averages. The explicit compensation for aerosol water is then

$$[\text{PM}_{2.5,\text{dry}}] = \frac{\langle[\text{PM}_{2.5,\text{dry}}]\rangle}{\langle b_{sp}(\text{RH})/f_v(\text{RH})\rangle} \cdot \frac{b_{sp}(\text{RH})}{f_v(\text{RH})} \qquad\qquad \text{Eq. A4}$$

where [] indicates concentration in µg m^{-3}. Uncertainties are a function of replicate weighing measurements ($\pm$ 4 µg), flow volume ($\pm$ 10%), %RH ($\pm$ 2.5), aerosol scatter ($\pm$ 5%), and κ_v ($\pm$ 0.05).

$$\left(\frac{\delta[\text{PM}_{2.5,\text{h}}]}{[\text{PM}_{2.5,\text{h}}]}\right)^2 \approx \left(\frac{\delta\text{PM}_{2.5}}{\text{PM}_{2.5}}\right)^2 + \left(\frac{\delta V}{V}\right)^2 + \left(\frac{\delta b_{sp}}{b_{sp}}\right)^2 + \left(\frac{\delta f_v}{f_v}\right)^2 \qquad\qquad \text{Eq. A5}$$

where

$$\left(\frac{\delta f_v}{f_v}\right)^2 = \frac{(f_v - 1)^2}{f_v^2}\left[\left(\frac{\delta\kappa}{\kappa}\right)^2 + \left(\frac{\delta\text{RH}}{\text{RH}\cdot(100 - \text{RH})}\right)^2\right] \qquad\qquad \text{Eq. A6}$$

The average relative 2-σ PM$_{2.5}$ uncertainty was 26% for dry hourly predictions, increasing with higher RH cutoffs. A cut-off of RH = 80% has been applied to our data, above which hygroscopic uncertainties, as well as total water mass, dominate.